Chemical Geology 255 (2008) 439–453

Contents lists available at ScienceDirect

Chemical Geology

journal homepage: www.elsevier.com/locate/chemgeo

# Eocene break-off of the Neo-Tethyan slab as inferred from intraplate-type mafic dykes in the Gaoligong orogenic belt, eastern Tibet

Yi-Gang Xu [a,*], Jiang-Bo Lan [a,b], Qi-Jun Yang [a,c], Xiao-Long Huang [a], Hua-Ning Qiu [a]

[a] Key Laboratory of Isotope Geochronology and Geochemistry, Guangzhou Institute of Geochemistry, Chinese Academy of Sciences, 510640 Guangzhou, China
[b] Graduate School of Chinese Academy of Sciences, Beijing 100039, China
[c] Guilin Institute of Technology, Guilin 541004, China

ARTICLE INFO

*Article history:*
Received 5 February 2008
Received in revised form 2 July 2008
Accepted 22 July 2008

Editor: B. Bourdon

*Keywords:*
Geochemistry
Mafic dykes
Intraplate type
Slab break-off
Eocene
Gaoligong
East Tibet

ABSTRACT

Eocene (40–42 Ma) basaltic dykes in the Gaoligong–Tengliang belt, eastern Tibet, are characterized by high $Na_2O$ (2–4%), in contrast with the widespread post-collisional potassic and ultrapotassic rocks in the Tibetan plateau. Despite the ubiquitous negative Nb anomalies, these dykes have relatively high Nb and Zr contents, making them distinct significantly from the Gangdese arc magmas. All these, together with the positive Nb anomaly in some samples, indicate an intraplate affinity for the Gaoligong–Tengliang dykes. Specifically, the Gaoligong dykes represent the asthenosphere-derived melts which has been contaminated to various degrees by the lithosphere mantle-derived melts, whereas the Tengliang samples were directly derived from an enriched lithosphere mantle. The thin lithosphere (<80 km) inferred from basalt geochemistry is unusual in Tibet, thus demanding a peculiar mechanism to thin lithosphere. A slab break-off model is preferred given the geochemical contrast between pre-40 Ma and post-40 Ma magmas in Tibet, and the temporal correlation among this intraplate magmatism, the termination of Gangdese arc magmatism and regional thermally-driven metamorphism. Therefore, the occurrence of intraplate-type magmas in the Gaoligong orogenic belt likely represents magmatic expression of the detachment of subducting Neo-Tethyan slab from the Indian continental plate during the Eocene. In the light of the slab break-off concept and thermo-mechanical modeling, the Eocene slab break-off furthermore suggests the onset of the India–Asia collision between 52 and 57 Ma.

© 2008 Elsevier B.V. All rights reserved.

## 1. Introduction

Petrogenetic understanding of magmas emplaced at different tectonic settings provides insights into thermal and physical relationships between crust/mantle melting and tectonic evolution (Wilson, 1989). Magmatism is widespread in Tibetan Plateau and has been used to tackle the tectonic evolution of this active collision zone (Coulon et al., 1986; Arnaud et al., 1992; Turner et al., 1993, 1996; Miller et al., 1999; Williams et al., 2001; Chung et al., 2003, 2005; Ding et al., 2003; Hou et al., 2004; Wang et al., 2005). While there is a consensus that magmatism reflects the response of the upper mantle and crust to the complex geodynamic evolution of this area, the relative role of northward subduction of Neo-Tethyan oceanic plate, slab rollback, slab break-off, continent–continent collision and subsequent detachment of sub-continental lithosphere in magmatic generation is a matter of hot debate (e.g., Chung et al., 2005). In particular, while the slab break-off must have taken place during the Indo-Asian collision, its timing and magmatic response to this event remain controversial. On the basis of a petrologic study on the Greater Himalayan metamorphic core, Kohn and Parkinson (2002) argued that decoupling of the oceanic lithosphere took place during the Eocene time. These authors suggested that late Eocene K-rich magmas in southeastern Tibet may represent magmatic expression of the slab break-off. A similar timing of slab break-off has been inferred by Chung et al. (2005) but on the basis of the termination age of the Gangdese arc magmatism. On the other hand, Mahéo et al. (2002) proposed that the Neogene magmatic and metamorphic evolution of the South Asian margin was controlled by slab break-off of the subducting Indian continental margin starting at about 25 Ma. This version of slab break-off model has been adopted by Hou et al. (2004) to explain mantle-derived ultrapotassic magmatism (17–25 Ma), which in turn triggered partial melting of the thickened lower crust to generate the Miocene (10–18 Ma) potassic adakites from southern Tibet.

If the timing of slab break-off reflects the diachronous evolution of the Tibetan plateau, then it is unclear why different magma compositions were produced through time across the Tibetan plateau by essentially the same trigger mechanism. The modeling by von Blanckenburg and Davies (1995) suggested that as the subducted oceanic plate breaks off, the underlying asthenosphere rises into the lithosphere break and impinges at the base of the thickened lithosphere of the overlying plate. This process will result in a heat supply that can

* Corresponding author. Tel.: +86 20 85290109; fax: +86 20 85290261.
*E-mail address:* yigangxu@gig.ac.cn (Y.-G. Xu).

0009-2541/$ – see front matter © 2008 Elsevier B.V. All rights reserved.
doi:10.1016/j.chemgeo.2008.07.016

induce melting and/or metamorphism of the overlying lithosphere, and eventually will induce decompression melting of the asthenosphere generating mafic magmas similar to oceanic island basalts (Turner et al., 1999; Maury et al., 2000; Ferrari, 2004). Whereas potassic magmatism is common in convergent zones, the occurrence of intraplate-type magmatism in such a setting is rather rare and thus has been considered diagnostic of slab break-off process (D'Orazio et al., 2001; Coulon et al., 2002; Ferrari, 2004). Herein we report the occurrence of Eocene intraplate-type mafic dykes in the Gaoligong–Tengliang belt in eastern Tibet and suggest that this provides the evidence for the break-off of the Neo-Tethyan plate during the Indo-Asian collision.

## 2. Geologic background and Cenozoic magmatic evolution in Tibet

The Tibetan Plateau is composed of a number of diverse exotic blocks that were accreted at different time. These blocks, namely high

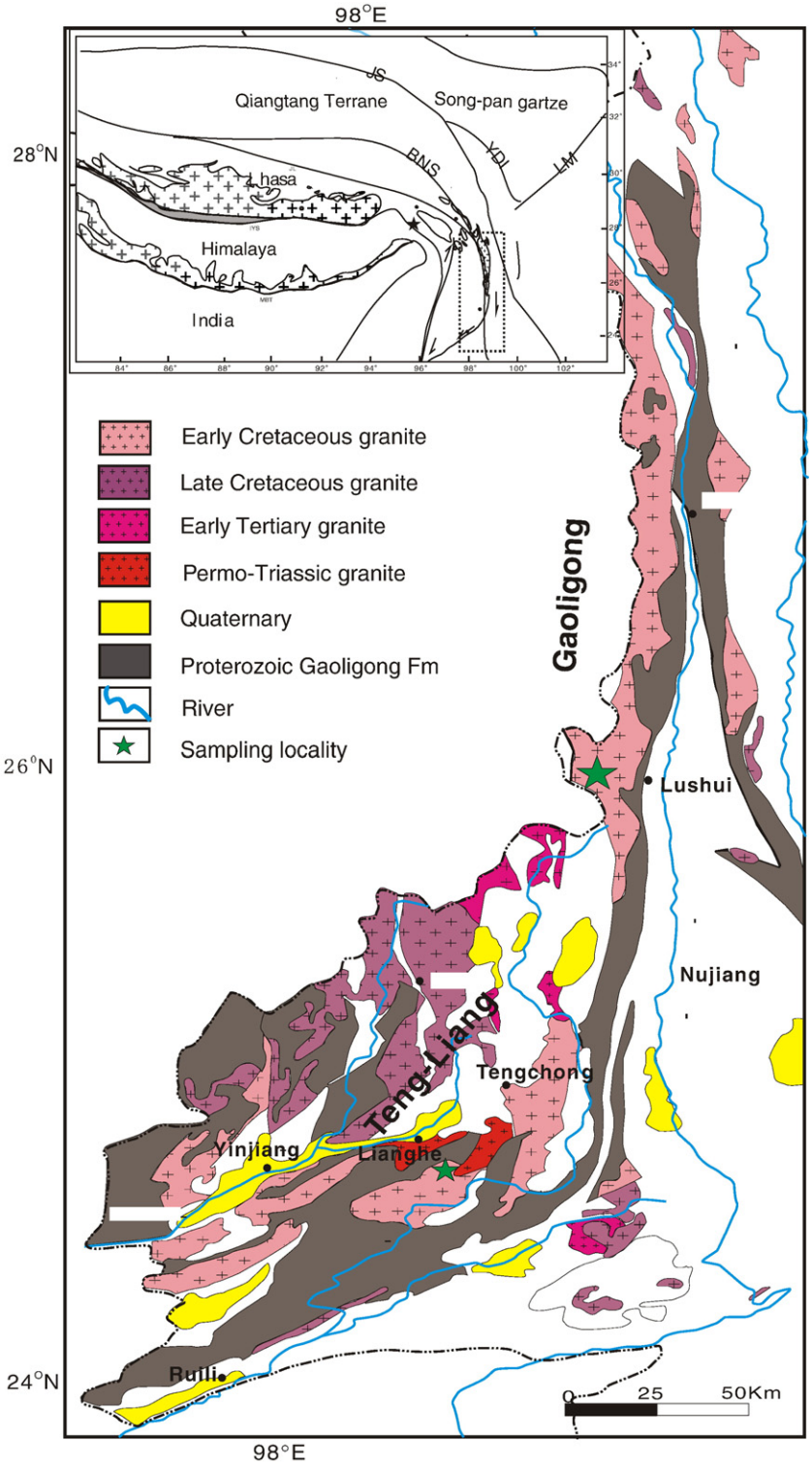


**Fig. 1.** Sketch map showing the major tectonic units of SW China and locations of the Gaoligong belt and sampling.

Himalaya, Lhasa and Qiangtang, are separated by different sutures (Fig. 1). The Yarlung-Tsanpo suture separated the Indian plate and Lhasa block. The latter is separated from the Qiangtang Terrane by the Banggong-Nujiang suture zone. The ages of these successive sutures decrease from north to south. For instance, the closure of the Meso-Tethys (leading to the Banggong-Nujiang suture) took place during the late Jurassic and early Cretaceous (Yin and Harrison, 2000; Kapp et al., 2005), and the closure of the neo-Tethys (leading to the Yarlung-Tsanpo suture) happened either in early Cenozoic (Yin and Harrison, 2000; Ding et al., 2003) or in Oligocene (Aitchison et al., 2007). The onset age of the Indo-Asian collision remains uncertain, largely because of different approaches used by different researchers and diverse definition of continental collision. For instance, Rowley (1996) considered the youngest marine strata of the Tethyan Himalaya in south-central Tibet as an indicator of the initiation of Indo-Asian collision in this region. Based on the paleogeographic analyses, he put forth a popular view that collision initiated in the northwestern Himalaya and progressed to the east. However, whether the disappearance of marine deposits marks the onset of collision has been questioned (Wu et al., 2008). Additional studies are needed to definitively test this diachronous collision model.

Two magmatic suites have been identified in the Lhasa terrane, namely southern Gangdese belt and northern magmatic belt (Coulon et al., 1986; Chung et al., 2005; Chu et al., 2006). The Gangdese belt, a huge quasi-continuous 2600-km long and 100-km wide belt, is composed of the Jurassic, late Cretaceous to Paleogene batholith ranging from gabbro to granite (Debon et al., 1986; Kapp et al., 2005; Wen et al., 2008). The northern magmatic belt is dominated by Jurassic–Early Cretaceous peraluminous or S-type granitic plutons (Xu et al., 1985; Lee et al., 2003). The boundary between the two magmatic belts is poorly defined. Recent investigation shows that the northern magmatic belt extends to rather south, overlapping the area occupied by the Gangdese plutons and the Linzizong volcanics (Chu et al., 2006).

The area covered by the north–south trending Gaoligong belt is situated to east of the eastern Himalayan Syntaxis (Fig. 1). This mountain range is 3000 m high and marks the divide between the Long Chuan River in the west and the Nu (Salween) River in the east. The basement in this area is composed of Precambrian high-grade metamorphic, late Paleozoic clastic sedimentary rocks and carbonates, and Mesozoic granitic intrusives. The Gaoligong–Tengliang region is geographically bounded by the Gaoligong Fault to the east. Recent SHRIMP Zircon U–Pb dating on the granitic batholiths reveals three episodes of magmatism in the Gaoligong–Tengliang area, which migrate form NE to SW (Yang et al., 2006; Xu et al., submitted for publication). The Gaoligong granites in the northeast were mainly emplaced during early Cretaceous (126–117 Ma), whereas the Tengliang granite, situated southwest of the Gaoligong belt, was emplaced in late Cretaceous (68–76 Ma). In the Yingjiang area, further west to the Tengliang area, Paleogene intrusions (53–55 Ma) were emplaced. Both Gaoligong and Tengliang granites are dominated by biotite-bearing, peraluminous and strongly peraluminous granite/leucogranite and granodiorites. Negative zircon $\varepsilon_{Hf}(t)$ values (−12 to −4) indicate a provenance of Proterozoic sedimentary source. They thus bear strong similarities to those in the northern magmatic belt in the Lhasa terrane in terms of lithology, geochemistry and emplacement age. However, the young plutons near the China-Burma boarder show I-type lithologic characteristics and have positive zircon $\varepsilon_{Hf}(t)$, somehow resembling the Gangdese batholith. This observation leads to the suggestion that the Gaoligong–Tengliang belt is a rotated, eastern extension of the Lhasa block (Xu et al., submitted for publication).

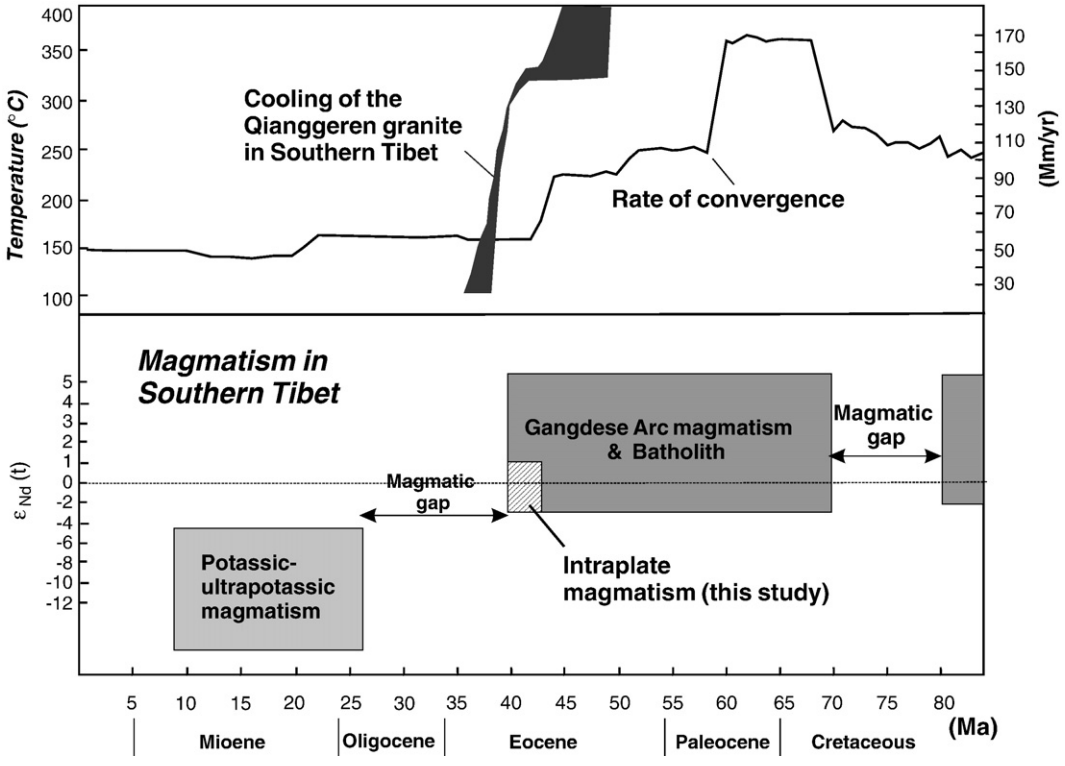


**Fig. 2.** Diagram summarizes the main episodes of magmatism in southern Tibet, cooling rate of the Qianggeren granite (He et al., 2007) and rate of convergence between India and Asia (right-hand ordinate) through the Late Cretaceous to Quaternary time periods (Lee and Lawver, 1995). The temporal scheme of the Gangdese magmatism is after Wen et al. (2008). Also shown for comparison are the $\varepsilon_{Nd}$ range of the Gangdese arc magmas (pre-40 Ma Gangdese batholith and Linzizong volcanics) and post-collisional (post-40 Ma) potassic and ultrapotassic magmas. Data sources: Coulon et al. (1986), Arnaud et al. (1992), Turner et al. (1996), Miller et al. (1999), Williams et al. (2001), Ding et al. (2003), Chung et al. (2003, 2005), Hou et al. (2004). Mo et al. (2007). Note that the emplacement of the Gaoligong–Tengliang intraplate dykes is temporally coincident with the onset of rapid cooling of the batholith and termination of the Gangdese arc magmatism.

### 2.1. Cenozoic magmatic evolution in Tibet

Cenozoic magmatism can be separated into three periods (Fig. 2). The first episode (70–40 Ma), termed Gangdese arc magmas, is marked by the widespread 5-km-thick Linzizong volcanic succession and the huge-scale granitoid batholiths in the southern Gangdese terrane (Chung et al., 2005; Mo et al., 2007). The $^{40}Ar/^{39}Ar$ and zircon U–Pb dating that indicate that the Linzizong eruption started at 65–69 Ma and continued to ~40 Ma (Zhou et al., 2004; He et al., 2007). Granitic rocks of the Gangdese batholith are mainly composed of granodiorite, quartz diorite, quartz monzonite and monzogranite, containing abundant mafic microgranular enclaves (Mo et al., 2007; Wen et al., 2008). U–Pb SHRIMP dating show that these granitoids were emplaced during 47–52 Ma (Schärer and Allègre, 1984, Mo et al., 2005; Dong et al., 2005; Wen et al., 2008). They have positive $\varepsilon_{Nd}(t)$ (+2.3–+8.3, Dong et al., 2005), similar to the values determined for the least crustally contaminated Lingzizong volcanic rocks (Mo et al., 2007).

The Gangdese arc magmatism was followed by a magmatic quiescence (40–26 Ma; Fig. 2), which may correspond to crustal thickening as the result of tectonic shortening. The compressional stress and thickening of continental lithosphere inhibited decompression melting in sublithospheric mantle. The magmatism resumed since ~26 Ma. These post-collisional magmas, largely emplaced during ~26 Ma and 10 Ma in southern Tibet, are composed of three types (Mo et al., 2007): (1) adakitic rocks emplaced during 25–12 Ma with a peak at 16 Ma; (2) a ~1300-km-long WNW–ESE belt (between 80°E and 91°E) of potassic–ultrapotassic volcanic rocks dated 26–10 Ma; and (3) some peraluminous granites of 24–18 Ma. Petrogenesis of these rocks are complex, involving partial melting of the thickened lower crust, subducted Indian mantle lithosphere, Tethyan ocean crust, terrigenous sediments, metasomatized Tibetan lithosphere and crustal level assimilation (Turner et al., 1993, Miller et al., 1999, Williams et al., 2001; Chung et al., 2003; Ding et al., 2003; Hou et al., 2004; Mo et al., 2006). One characteristic of these rocks are their highly negative $\varepsilon_{Nd}(t)$ values that contrast with the generally positive $\varepsilon_{Nd}(t)$ values observed in the Gangdese arc magmas (Fig. 2). The ultrapotassic rocks located to west of the longitude of 87°E show Sr–Nd isotopic compositions that resemble that of the Indian crustal basement. This has been taken as evidence for the subduction of the Indian continental plate underneath the Lhasa Terrane since the Oligocene (Zhao et al., 2003; Guo et al., 2007).

## 3. Samples and analytical methods

Mafic dykes were collected in late Cretaceous granites near Lushui-Pianma and near Lianghe (Fig. 1). The Lushui-Pianma mafic dykes intruded the late Cretaceous Gaoligong granites (68–76 Ma). The Lianghe samples were collected from dykes that intruded ~54 Ma granites at Nangsong. The width of these dykes range from 1 m to 6 m. The contact between dyke and granite is generally sharp. These samples show holocrystalline and/or porphyritic-seriate textures, with phenocrysts consisting dominantly of clinopyroxene and plagioclase. The mineral assemblage of the groundmass is similar to that of phenocrysts but has a higher population of opaque minerals and apatite. The samples experienced some degrees of alteration showing replacement of pyroxene by hornblende or serpentine. While most samples do not have cumulate textures and so may represent magma compositions, one picritic sample (GLS-21) displays a cumulate texture. This sample show severe alteration and only traces of olivine and clinopyroxene are preserved.

Ten samples were sawed into slabs and the central parts were used for bulk-rock analyses. The rocks were crushed in a steel mortar and ground in a steel mill. Bulk-rock abundances of major elements were determined using an X-ray fluorescence spectrometer (XRF) on glass disks at the Guangzhou Institute of Geochemistry, Chinese Academy of Sciences (GIGCAS), following analytical procedures described by Goto and Tatsumi (1996). A pre-ignition was used to determine the loss on ignition (LOI) prior to major element analyses. Analytical uncertainties for majority of major elements analyzed were estimated at smaller than 1% from repeatedly analyzed U.S.G.S. standards BHVO-2, MRG-1 (basalt) and W-2 (diabase). Bulk-rock trace-element data [rare earth elements (REE), Sc, Ti, V, Cr, Cs, Sr, Y, Ba, U, Rb, Th, Pb, Zr, Hf, Nb, Ta] were obtained by inductively coupled plasma-mass spectrometry (ICP-MS) at GIGCAS, following the analytical procedures described by Xu (2002). Precision for REE and HFSE is estimated to be 5% from repeatedly analyzed U.S.G.S. standards BHVO-1 and W-2 (Xu, 2002).

For Sr–Nd isotopic analyses, sample powders (~100 mg) were dissolved in distilled HF-$HNO_3$ Savillex screwtop Teflon beakers at 150 °C overnight. Sr and REE were separated on columns made of Sr and REE resins (4,4′(5′)-di-*t*-butylcyclohexano18-crown-6) of the Eichrom Company using 0.1% $HNO_3$ as elutant. Separation of Nd from the REE fractions was carried out on HDEHP (phosphoric acid, bis (2-ethylhexy) ester) columns with a 0.18 N HCl elutant. The isotopic analyses were performed using a Micromass Isoprobe Multi-Collector ICPMS at GIGCAS. Measured Sr and Nd isotopic ratios were normalized using a $^{86}Sr/^{88}Sr$ value of 0.1194 and a $^{146}Nd/^{144}Nd$ value of 0.7219, respectively. The Sr and Nd blanks during the period of analyses are 0.5 ng and 0.3 ng, respectively. Analyses of standards during the period of analysis are as follows: NBS987 gave $^{87}Sr/^{86}Sr = 0.710243 \pm 14$ ($2\sigma$); Shin Etou gave $^{143}Nd/^{144}Nd = 0.512124 \pm 11$ ($2\sigma$), equivalent to a value of 0.511860 for the La Jolla international standard (Tanaka et al., 2004).

The $^{40}Ar/^{39}Ar$ dating was carried out at GIGCAS by using GV5400 mass spectrometer following analytical procedures described by Qiu and Jiang (2007). Argon gas was extracted from the sample by step-

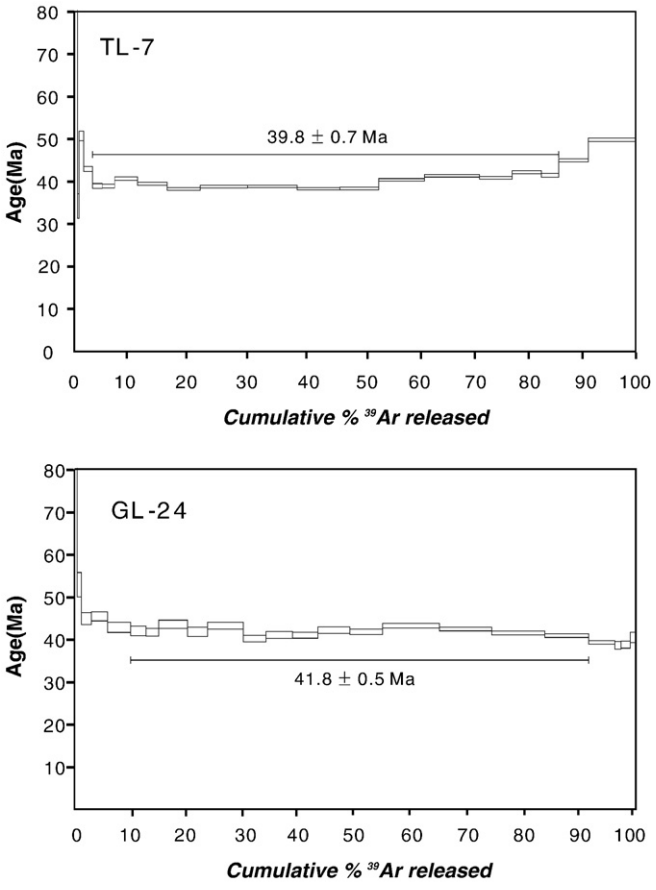


**Fig. 3.** Ar–Ar age spectra of the whole rocks of the Gaoligong–Tengliang mafic dykes.

heating using MIR10 $CO_2$ continuing laser. The released gases were purified by two Zr/Al getter pumps operated for 5 to 8 min at room temperature and ~450 °C respectively. The background of the sample hold is lower than 2 mV pre-experiment, while the signal of the sample is mostly between 40–200 mV. The $^{40}Ar/^{39}Ar$ dating results are calculated and plotted using the ArArCALC software by Koppers (2002). The *J*-value was 0.00955 as determined by ZBH-2506 biotite (132 Ma) flux monitors.

## 4. Results

### 4.1. Ar–Ar geochronology

Two samples (GL-24, TL-7) were selected for $^{40}Ar/^{39}Ar$ dating. The plateau ages for these two samples are 39.7±0.7 Ma and 41.8±0.5 Ma (Fig. 3), respectively, and represent more than 90% cumulative $^{39}Ar$ released. All the steps were strongly enriched in radiogenic $^{40}Ar$ as a result of radiogenic decay from potassium (Table 1). This suggests that the mafic dykes were emplaced at 40–42 Ma in the Gaoligong–Tengliang region. This emplacement age is roughly equivalent to the time at which the Linzizong volcanism ended (~40 Ma; Zhou et al., 2004; Chung et al., 2005), i.e., the cessation of the Gangdese arc magmatism at ~40 Ma (Fig. 2).

### 4.2. Geochemistry

Elemental and isotopic compositions are listed in Table 2. The Gaoligong–Tengliang mafic rocks have $SiO_2$ contents ranging from 46% to 57% with the majority between 46% and 50%. Their Mg values (0.51–0.76) suggest that they have experienced minor to moderate differentiation. In the plot of $Na_2O+K_2O$ against $SiO_2$ (Fig. 4a), the Gaoligong–Tengliang mafic rocks straddle the alkali basalt-tholeiite boundary. Although plotted overlapping with the Linzizong volcanic rocks, the Gaoligong samples display a more restricted range of compositions with most corresponding to basalts (Figs. 4a, 5a). Moreover, these rocks are characterized by relatively high $Na_2O$ but low $K_2O$ contents, making them distinct from the widespread post-collision potassic–ultrapotassic rocks and Gangdese arc magmas in the Tibetan plateau (Fig. 4a–b).

The Gaoligong–Tengliang dykes are more basic than the Linzizong volcanics (Fig. 5). The sample GLS-21 has the highest MgO content (~20%), consistent with its cumulate texture. The remaining samples

**Table 1**
$^{40}Ar/^{39}Ar$ dating results of the Gaolingong mafic dikes

| Laser output energy (W) | 36 Ar(a) (mV) | 38 Ar(cl) (mV) | 39 Ar(k) (mV) | 40 Ar(r) (mV) | Age (Ma) ±2σ (Ma) | 40 Ar(r) (%) | 39Ar(k) (%) |
|---|---|---|---|---|---|---|---|
| TL-7 (whole rock) | T1=39.68±0.72 Ma | | T2=41.43±0.15 Ma | | T3=39.03±1.63 Ma | T4=39.69±1.75 Ma | |
| 3 | 0.00003 | 0.000001 | 0.00231 | 0.01308 | 112.9±2.7 | 62.3 | 0.57 |
| 3 | 0.00001 | 0 | 0.00111 | 0.00186 | 34.2±2.9 | 55.41 | 0.27 |
| 3.5 | 0.00001 | 0 | 0.00343 | 0.00855 | 50.8±1.2 | 65.97 | 0.84 |
| 4 | 0.00002 | 0 | 0.00637 | 0.01343 | 43±0.6 | 71.56 | 1.57 |
| 4.5 | 0.00002 | 0 | 0.00708 | 0.01353 | 39±0.6 | 73.93 | 1.74 |
| 5 | 0.00002 | 0 | 0.00893 | 0.01704 | 38.9±0.5 | 75.81 | 2.2 |
| 6 | 0.00003 | 0 | 0.01662 | 0.03317 | 40.7±0.5 | 78.55 | 4.09 |
| 7 | 0.00003 | 0.000001 | 0.02147 | 0.04155 | 39.5±0.4 | 81.05 | 5.29 |
| 8 | 0.00003 | 0.000002 | 0.02385 | 0.04472 | 38.3±0.3 | 85.5 | 5.88 |
| 10 | 0.00003 | 0.000007 | 0.03401 | 0.06475 | 38.8±0.3 | 86.74 | 8.38 |
| 11 | 0.00003 | 0.000008 | 0.0359 | 0.06837 | 38.8±0.3 | 87.59 | 8.84 |
| 12 | 0.00003 | 0.000008 | 0.03108 | 0.05842 | 38.3±0.3 | 88.1 | 7.66 |
| 13 | 0.00002 | 0.000006 | 0.02799 | 0.05266 | 38.4±0.3 | 89.42 | 6.9 |
| 15 | 0.00002 | 0.000006 | 0.03293 | 0.06525 | 40.4±0.3 | 90.13 | 8.11 |
| 17 | 0.00003 | 0.000011 | 0.03981 | 0.08078 | 41.4±0.3 | 91 | 9.81 |
| 18 | 0.00002 | 0.000005 | 0.02384 | 0.0478 | 40.9±0.3 | 90.54 | 5.87 |
| 20 | 0.00001 | 0.000005 | 0.0211 | 0.04367 | 42.2±0.3 | 93.28 | 5.2 |
| 21 | 0.00001 | 0.000003 | 0.01248 | 0.02539 | 41.5±0.5 | 92.96 | 3.08 |
| 30 | 0.00001 | 0.000008 | 0.02137 | 0.04721 | 45±0.4 | 92.64 | 5.26 |
| 100 | 0.00003 | 0.000017 | 0.03424 | 0.08395 | 49.9±0.4 | 91.23 | 8.44 |
| GL-24 (whole rock) | T1=41.78±0.52 Ma | | T2=42.23±0.21 Ma | | T3=41.22±1.33 Ma | T4=41.30±1.34 Ma | |
| 3 | 0.00009 | 0.000002 | 0.00152 | 0.00688 | 91.±7.4 | 21.32 | 0.47 |
| 3.5 | 0.00005 | 0 | 0.00239 | 0.00619 | 52.8±2.9 | 27.99 | 0.75 |
| 4 | 0.00006 | 0 | 0.00562 | 0.01234 | 44.8±1.4 | 41.23 | 1.76 |
| 5 | 0.00009 | 0 | 0.00928 | 0.02063 | 45.4±1.1 | 44.07 | 2.9 |
| 6 | 0.00011 | 0 | 0.01308 | 0.02741 | 42.8±1.2 | 45.64 | 4.09 |
| 6.5 | 0.00007 | 0 | 0.00885 | 0.01819 | 42±1.1 | 46.17 | 2.77 |
| 7 | 0.00005 | 0 | 0.00717 | 0.01461 | 41.6±0.9 | 48.43 | 2.24 |
| 8 | 0.00013 | 0 | 0.01656 | 0.03531 | 43.5±0.9 | 48.07 | 5.18 |
| 8.5 | 0.0001 | 0 | 0.01131 | 0.02311 | 41.7±1.1 | 43.89 | 3.54 |
| 9.5 | 0.00013 | 0.000001 | 0.02044 | 0.04327 | 43.2±0.8 | 53.47 | 6.4 |
| 10 | 0.00008 | 0 | 0.01291 | 0.02536 | 40.1±0.8 | 50.93 | 4.04 |
| 11 | 0.00009 | 0 | 0.01494 | 0.03 | 41±0.8 | 53.59 | 4.68 |
| 12 | 0.00007 | 0 | 0.01446 | 0.029 | 41±0.7 | 57.14 | 4.53 |
| 14 | 0.00011 | 0 | 0.01812 | 0.0374 | 42.1±0.8 | 54.09 | 5.67 |
| 16 | 0.00009 | 0 | 0.0188 | 0.03844 | 41.7±0.6 | 59.35 | 5.88 |
| 18 | 0.00013 | 0 | 0.03235 | 0.06845 | 43.2±0.5 | 64.53 | 10.13 |
| 20 | 0.00009 | 0 | 0.02978 | 0.06186 | 42.4±0.4 | 70.36 | 9.32 |
| 22 | 0.00009 | 0 | 0.03003 | 0.06094 | 41.4±0.5 | 69.87 | 9.4 |
| 25 | 0.00006 | 0 | 0.02511 | 0.05021 | 40.8±0.4 | 74.14 | 7.86 |
| 30 | 0.00003 | 0.000002 | 0.01479 | 0.02841 | 39.2±0.4 | 74.99 | 4.63 |
| 31 | 0 | 0 | 0.00354 | 0.00669 | 38.6±0.9 | 84.1 | 1.11 |
| 40 | 0.00001 | 0 | 0.00521 | 0.00986 | 38.7±0.8 | 79.06 | 1.63 |
| 50 | 0.00001 | 0 | 0.00326 | 0.00645 | 40.4±1.3 | 68.1 | 1.02 |

T1 — Plateau age; T2 — molten age; T3 — isochron; T4 — inverted isochron.

**Table 2**
Major (wt.%), trace element (ppm) and Sr–Nd isotopic composition of the Gaoligong mafic dikes

| | Lianghe | | | | Lushui | | | | | |
|---|---|---|---|---|---|---|---|---|---|---|
| | TL-2 | TL-3 | TL-4 | TL-7 | GL-8 | GL-24 | GL-22 | GLS-16 | GLS-21 | GLS-27 |
| $SiO_2$ | 49.14 | 49.51 | 51.31 | 57.31 | 49.8 | 46.2 | 49.6 | 48.53 | 42.35 | 50.7 |
| $Al_2O_3$ | 16.08 | 16.16 | 16.78 | 17.59 | 15.43 | 16.3 | 17 | 16.19 | 9.4 | 14.05 |
| $Fe_2O_3T$ | 10.87 | 10.86 | 10.18 | 7.84 | 9.53 | 13.4 | 11.7 | 12.89 | 14.51 | 13.31 |
| MgO | 7.09 | 6.9 | 3.9 | 3.46 | 8.22 | 6.22 | 5.2 | 6.37 | 19.51 | 6.27 |
| $Na_2O$ | 3.1 | 3.18 | 3.38 | 2.99 | 1.95 | 2.76 | 3.98 | 3.46 | 0.32 | 3.64 |
| $K_2O$ | 1.34 | 1.37 | 1.68 | 1.55 | 2.15 | 1.13 | 0.51 | 1.5 | 0.16 | 0.26 |
| CaO | 7.12 | 7.27 | 7.87 | 5.89 | 8.33 | 7.88 | 7.69 | 7.72 | 7.12 | 8.24 |
| $TiO_2$ | 1.38 | 1.41 | 1.3 | 0.82 | 1.22 | 2.47 | 2.1 | 2.42 | 1 | 1.57 |
| $P_2O_5$ | 0.28 | 0.29 | 0.31 | 0.12 | 0.2 | 0.26 | 0.39 | 0.42 | 0.09 | 0.17 |
| MnO | 0.15 | 0.16 | 0.51 | 0.11 | 0.14 | 0.18 | 0.18 | 0.19 | 0.2 | 0.21 |
| LOI | 3.7 | 3.12 | 2.58 | 2.51 | 2.63 | 3.08 | 1.8 | 0.59 | 5.8 | 2.25 |
| Total | 100.25 | 100.22 | 99.79 | 100.17 | 99.6 | 99.8 | 100 | 100.26 | 100.46 | 100.68 |
| Mg# | 60.3 | 59.7 | 47.2 | 50.7 | 66.8 | 52.1 | 50.9 | 53.5 | 75.8 | 52.3 |
| Q | 2.7 | 2.6 | 6.1 | 16.9 | 3.6 | 2.5 | 3.4 | 0.3 | 0.0 | 6.4 |
| Or | 9.0 | 9.1 | 11.2 | 10.1 | 14.2 | 7.8 | 3.4 | 9.9 | 1.1 | 1.8 |
| Ab | 31.5 | 32.1 | 34.2 | 29.5 | 19.5 | 29.0 | 40.2 | 34.8 | 3.4 | 37.4 |
| An | 29.4 | 29.0 | 28.9 | 31.3 | 30.1 | 33.7 | 30.4 | 27.1 | 27.9 | 24.3 |
| Di | 3.0 | 3.7 | 8.0 | 0.0 | 8.3 | 0.7 | 1.8 | 3.3 | 7.8 | 12.7 |
| Hy | 20.7 | 19.6 | 8.2 | 10.5 | 21.1 | 19.8 | 15.2 | 18.1 | 51.4 | 13.5 |
| Ol | 0.0 | 0.0 | 0.0 | 0.0 | 0.0 | 0.0 | 0.0 | 0.0 | 6.0 | 0.0 |
| Il | 0.3 | 0.3 | 0.9 | 0.2 | 0.2 | 0.3 | 0.3 | 0.3 | 0.4 | 0.4 |
| Ti | 2.9 | 2.9 | 1.7 | 0.0 | 2.5 | 5.6 | 4.5 | 5.2 | 1.9 | 3.2 |
| Ap | 0.7 | 0.7 | 0.7 | 0.3 | 0.5 | 0.6 | 0.9 | 1.0 | 0.2 | 0.4 |
| Cr | 132.00 | 151.20 | 157.00 | 13.25 | 314.50 | 118.00 | 58.40 | 98.73 | 1145.20 | 77.54 |
| Ni | 84.35 | 142.40 | 71.29 | 9.49 | 138.60 | 67.10 | 50.50 | 67.35 | 696.80 | 49.44 |
| Sc | 20.68 | 21.30 | 20.58 | 17.80 | 19.66 | 19.20 | 21.10 | 21.53 | 27.23 | 40.31 |
| V | 137.20 | 139.80 | 161.60 | 190.20 | 162.00 | 201.00 | 182.00 | 194.90 | 186.20 | 324.70 |
| Co | 40.63 | 62.39 | 62.38 | 21.16 | 37.06 | 38.20 | 34.70 | 39.97 | 82.71 | 44.12 |
| Cu | 34.86 | 34.79 | 28.30 | 34.60 | 50.78 | 74.80 | 72.20 | 65.78 | 204.20 | 169.90 |
| Zn | 85.98 | 123.40 | 106.60 | 82.06 | 71.45 | 105.00 | 115.00 | 118.80 | 84.88 | 101.90 |
| Ga | 18.00 | 17.65 | 18.75 | 19.42 | 16.89 | 19.30 | 21.10 | 20.43 | 11.46 | 16.97 |
| Ge | 1.66 | 1.98 | 1.83 | 1.67 | 1.48 | 1.84 | 1.61 | 1.86 | 1.74 | 2.18 |
| Cs | 2.39 | 0.31 | 0.32 | 16.81 | 44.58 | 6.47 | 3.02 | 3.12 | 0.59 | 0.89 |
| Rb | 27.62 | 29.76 | 37.75 | 157.20 | 206.10 | 49.40 | 28.00 | 29.64 | 5.82 | 6.79 |
| Sr | 387.4 | 391.8 | 461.2 | 235.3 | 260.7 | 405.0 | 389.0 | 370.5 | 4.9 | 232.9 |
| Ba | 385.8 | 411.4 | 529.6 | 215.5 | 145.7 | 214.0 | 153.0 | 233.9 | 9.8 | 98.8 |
| Zr | 123.0 | 127.5 | 171.1 | 118.2 | 134.3 | 193.0 | 220.0 | 215.4 | 63.9 | 129.7 |
| Hf | 3.55 | 3.63 | 4.86 | 4.08 | 3.73 | 5.46 | 6.24 | 6.46 | 2.20 | 4.30 |
| Nb | 12.06 | 12.75 | 14.30 | 8.57 | 9.74 | 18.10 | 19.70 | 19.87 | 4.20 | 11.63 |
| Ta | 0.75 | 0.79 | 0.89 | 0.57 | 0.83 | 1.34 | 1.33 | 1.46 | 0.32 | 0.89 |
| Y | 23.81 | 31.52 | 43.75 | 24.36 | 21.75 | 33.30 | 37.10 | 40.22 | 20.61 | 36.97 |
| La | 25.05 | 27.42 | 41.29 | 19.19 | 18.91 | 16.60 | 24.10 | 25.95 | 5.78 | 16.55 |
| Ce | 46.79 | 50.10 | 71.04 | 38.80 | 37.68 | 43.10 | 54.80 | 59.50 | 12.79 | 34.08 |
| Pr | 5.74 | 6.01 | 8.38 | 4.72 | 4.73 | 6.43 | 7.55 | 8.35 | 1.82 | 4.44 |
| Nd | 22.49 | 24.50 | 33.01 | 18.61 | 18.51 | 27.90 | 33.10 | 36.53 | 8.85 | 19.85 |
| Sm | 4.52 | 4.70 | 6.07 | 4.12 | 4.10 | 6.32 | 6.93 | 7.80 | 2.49 | 4.79 |
| Eu | 1.45 | 1.59 | 1.76 | 1.05 | 1.25 | 2.11 | 2.19 | 2.51 | 0.78 | 1.50 |
| Gd | 4.80 | 5.30 | 6.30 | 4.25 | 4.20 | 6.63 | 7.39 | 8.39 | 3.45 | 6.35 |
| Tb | 0.74 | 0.85 | 1.02 | 0.73 | 0.71 | 1.05 | 1.19 | 1.32 | 0.59 | 1.06 |
| Dy | 4.48 | 5.02 | 6.11 | 4.52 | 3.93 | 6.15 | 6.72 | 7.72 | 3.79 | 6.59 |
| Ho | 0.83 | 1.04 | 1.24 | 0.89 | 0.82 | 1.30 | 1.35 | 1.52 | 0.78 | 1.38 |
| Er | 2.16 | 2.61 | 3.35 | 2.44 | 2.40 | 3.58 | 3.34 | 3.82 | 2.00 | 3.54 |
| Tm | 0.32 | 0.36 | 0.45 | 0.36 | 0.35 | 0.54 | 0.48 | 0.56 | 0.30 | 0.54 |
| Yb | 1.87 | 2.18 | 2.69 | 2.24 | 2.13 | 3.33 | 2.89 | 3.38 | 1.80 | 3.14 |
| Lu | 0.26 | 0.33 | 0.41 | 0.34 | 0.33 | 0.52 | 0.43 | 0.50 | 0.26 | 0.47 |
| Pb | 5.33 | 6.23 | 9.12 | 17.93 | 8.25 | 1.93 | 6.56 | 7.22 | 2.20 | 5.21 |
| Th | 5.49 | 5.89 | 7.31 | 8.22 | 5.58 | 1.82 | 2.74 | 3.29 | 0.88 | 4.57 |
| U | 0.70 | 0.79 | 0.79 | 1.37 | 0.88 | 0.35 | 0.53 | 0.55 | 0.18 | 0.84 |
| $^{87}Sr/^{86}Sr$ | | | | 0.714975 | 0.707939 | 0.707898 | 0.706815 | 0.706702 | | 0.708818 |
| $(^{87}Sr/^{86}Sr)i$ | | | | 0.713876 | 0.706639 | 0.707697 | 0.706697 | 0.706571 | | 0.70877 |
| $2\sigma$ | | | | 14 | 16 | 8 | 13 | 11 | | 20 |
| $^{143}Nd/^{144}Nd$ | | | | 0.512424 | 0.512461 | 0.512585 | 0.512604 | 0.512531 | | 0.512511 |
| $2\sigma$ | | | | 12 | 6 | 6 | 9 | 7 | | 9 |
| TDM (Ga) | | | | 1.39 | 1.32 | 1.13 | 0.96 | 1.12 | | 1.43 |
| $(^{143}Nd/^{144}Nd)i$ | | | | 0.512389 | 0.512426 | 0.512549 | 0.512571 | 0.512497 | | 0.512473 |
| $\varepsilon Nd$ | | | | −3.85 | −3.13 | −0.73 | −0.3 | −1.74 | | −2.21 |

define a compositional trend different from that of the Linzizong volcanics. Specifically, they show a negative correlation between $Al_2O_3$ and MgO, which contrasts with the positive correlation defined by the Linzizong volcanics. Moreover, they have higher $TiO_2$ and Nb contents than the Linzizong volcanics. All these rule out a direct petrogenetic link between the two suites.

The primitive mantle-normalized trace-element distribution patterns of the most Gaoligong–Tengliang dykes are characterized by

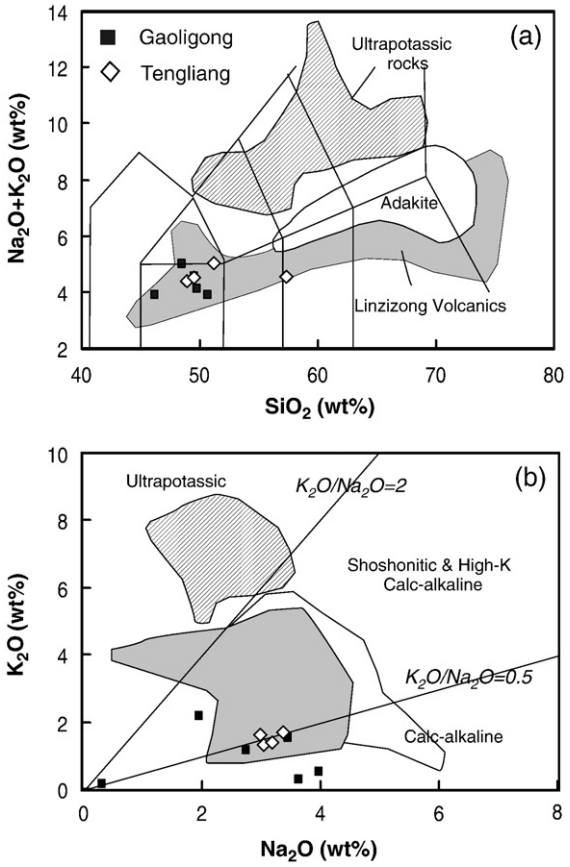


**Fig. 4.** (a) Plots of total alkalis versus silica (TAS) of the Gaoligong mafic dykes. (b) $K_2O$ versus $Na_2O$ plot. The field of the Linzizong volcanic is after Mo et al. (2007). The fields for ultrapotassic and adakitic rocks in southern Tibet are from Chung et al. (2005).

enrichment of large ion lithophile elements (LILE) and depletion of high field strength elements (HFSE) (Fig. 6). It is noted that the negative anomalies of Nb, Ta and Ti are less pronounced in the Gaoligong samples than in the Tengliang samples. The extent of Nb-depletion in the Gaoligong–Tengliang dykes is much less significant than the typical arc magmatism (Fig. 6). The weak negative Sr anomalies in these samples also contrast with pronounced positive Sr anomaly in arc magmas (Fig. 6). More importantly, sample GL-24 shows no anomaly of Nb, Ta and Ti, but depletions in Th and U (Fig. 6a).

Initial Sr–Nd isotopic ratios were calculated for the emplacement age of 40 Ma. The Gaoligong–Tengliang mafic dykes have highly radiogenic $^{87}Sr/^{86}Sr(t)$ ranging from 0.7065 to 0.7139 and unradiogenic $^{143}Nd/^{144}Nd$ with initial $\varepsilon_{Nd}(t)$ values ranging from −0.30 to −3.9 (Fig. 7). Overall, isotopically they are intermediate between the Linzizong volcanics and the Gaoligong batholith (Fig. 7).

## 5. Discussion

### 5.1. Intraplate-type magmatism in the Gaoligong orogenic belt

Although most of the Gaoligong–Tengliang mafic dykes display negative Nb–Ta anomalies, they show the following characteristics, which are different from typical arc magmas, but resemble those produced in intraplate settings.

(1) The Gaoligong–Tengliang mafic dykes are composed predominantly of basalts, in contrast with dominant andesite of arc magmatic series. Relatively high $Na_2O$ and low $K_2O$ contents in these rocks also make them distinct from the post-collisional potassic and ultrapotassic rocks in southern Tibet.

(2) $TiO_2$ and Nb abundance in the studied rocks ranges from 1.3 to 2.5% and 8.5 to 20 ppm, respectively, considerably higher than typical intra-oceanic arc basalts (<1% and <2 ppm, Martin et al., 2005) and subduction-related to calc-alkaline andesites (Fig. 5e). Moreover, their extent of Nb-depletion is much less significant than the typical arc magmatism (Fig. 6). The weak negative Sr anomalies in these samples also contrast with pronounced positive Sr anomaly in arc magmas (Fig. 6).

(3) The Gaoligong–Tengliang samples have relatively higher Zr contents (118–220 ppm) than typical arc magmas (<50 ppm). In the plot of Zr–Zr/Y, they are plotted within the field of within-plate basalts (Fig. 8a). These samples also show distinctly lower Zr/Nb rations than those of subduction-related lavas (VAB in Fig. 8b).

(4) The intraplate type of the Gaoligong–Tengliang mafic dykes is further highlighted by a small number of samples which show no Nb anomaly (e.g., GL-24, Fig. 6). Specifically, the sample GL-24 has Nb/La greater than 1 and Nb/U (51.7), which are in good agreement with the averaged values of OIB and MORB (Hofmann, 1997; Fig. 8b).

We thus conclude that the Gaoligong–Tengliang mafic dykes are of intraplate-type basalts, rather than arc-related magmas. They were most likely related to the asthenospheric upwelling during the Eocene in the studied area. The development of Nb–Ta depletion may have resulted either from assimilation of crustal component(s) during magmatic ascent and/or magma chamber processes, or mixing with melts derived from enriched lithospheric mantle. Distinction between these alternatives will be discussed in the following section.

### 5.2. Lithosphere mantle–asthenosphere interaction

$\varepsilon_{Nd}$ values of the Gaoligong–Tengliang dykes correlate positively with Nb/La, but negatively with $SiO_2$ and MgO (Fig. 9). These relationships are consistent with mixing of two isotopically distinct components. As argued above, one component with relatively high $\varepsilon_{Nd}$ and high Nb/La is plausibly from the asthenosphere. Another mixing component, characterized by low $\varepsilon_{Nd}$ and Nb/La (Fig. 9a), may be either from the crust or the lithospheric mantle, or both.

The positive correlation between Nb/La and $\varepsilon_{Nd}$ (Fig. 9a) and the negative correlation between $SiO_2$ and $\varepsilon_{Nd}$ (Fig. 9b) are consistent with crustal contamination processes. Country rocks in the studied area include Proterozoic sedimentary rocks and Mesozoic granitic batholith. The Proterozoic Chongshan Formation, characterized by a positive $\varepsilon_{Nd}$ (Yang et al., 2006), cannot act as a suitable contaminant. The Mesozoic granites show negative $\varepsilon_{Nd}$ (−12) and pronounced negative Nb anomaly (Nb/La as low as 0.3). These rocks thus can be potential contaminants. Calculation suggests that up to 40% contamination of crustal components can account for the compositional variation observed in the Gaoligong–Tengliang dykes. However, such a high extent of assimilation of felsic crust in the studied dykes will not maintain their basaltic compositions. On the other hand, if the upper crust was involved in the genesis of the studied dykes, the most contaminated samples with the lowest $\varepsilon_{Nd}$ would also display the lowest Sm/Nd and MgO, because upper crust is generally characterized by LILE-enrichment (low Sm/Nd) and low MgO contents. The negative correlation between MgO and $\varepsilon_{Nd}$ (Fig. 9c) and Sm/Nd (Fig. 9d) are opposite to the trends expected by crustal contamination model. As such, crustal contamination cannot adequately account for geochemistry of the Gaoligong–Tengliang basaltic dykes.

The Tengliang samples exhibit well-developed Nb–Ta depletions (Fig. 6b). The Nb/La ratios in these samples remain virtually unchanged irrespective of MgO and $SiO_2$ contents (Fig. 9e, f). This suggests the Nb–Ta deficits in the Tengliang samples inherited that of the source, rather than from crustal contamination. The possible

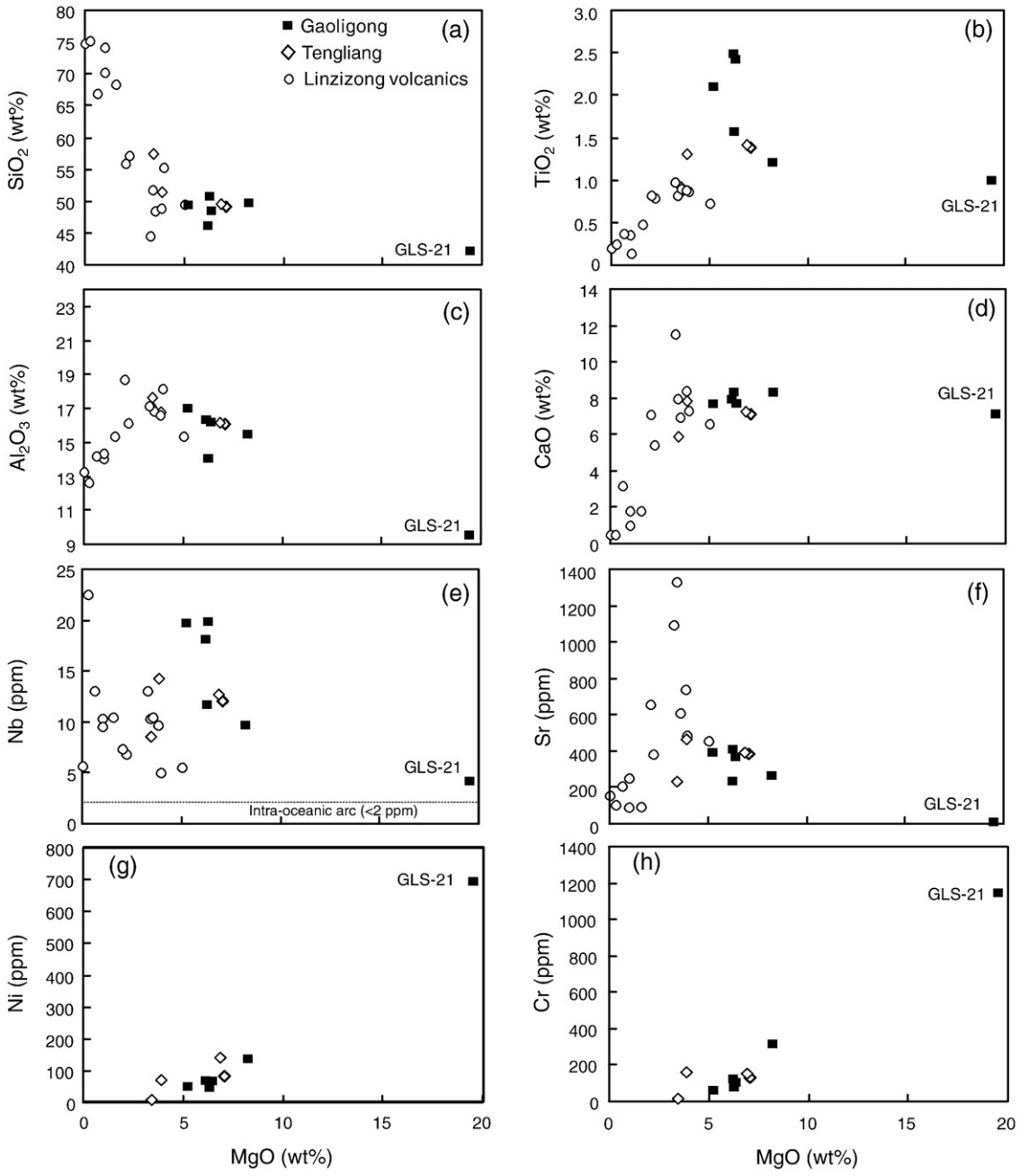


**Fig. 5.** Variation of $SiO_2$, $TiO_2$, $Al_2O_3$, CaO, Ni and Cr versus MgO for the Gaoligong–Tengliang mafic dykes. Also shown are the data for the Linzizong volcanics (Mo et al., 2007).

candidate for this source is the metasomatized lithospheric mantle, which is likely in the form of pyroxenite-vein plus refractory peridotites. Recent experiments demonstrated that melting of pyroxenite-bearing peridotites is capable of producing Si-rich basalts (Hirschmann et al., 2003; Kogiso et al., 2004), with geochemical characteristics similar to those for the Tengliang samples. $T_{DM}$ (>1.0 Ga; Table 1) further suggests an old magma source. It can thus be concluded that the Tengliang dykes were likely derived from by the continental lithospheric mantle (CLM) which has been metasomatized by slab-derived fluids during previous subductions. In Fig. 9a and b, Tengliang and Gaoligong samples define a coherent correlation, with the Tengliang samples forming an end of the correlation. Therefore the Gaoligong samples likely represent melts derived from asthenosphere, mixed with melts from an enriched lithospheric mantle.

### 5.3. Evidence for a shallow asthenospheric mantle source

The most primitive rocks of the Gaoligong–Tengliang mafic dykes are q-hy-normative. Compared to the experimental results on partial melting of anhydrous mantle peridotites (Takahashi and Kushiro, 1983; Hirose and Kushiro, 1993), such a petrologic feature would indicate a pressure of magma segregation of 15–20 kbar. This relatively shallow depth of melt extraction is further supported by the REE modeling. Fig. 10a shows the [Sm/Yb]*n* versus [La/Sm]*n* ratios for the Gaoligong–Tengliang samples, together with the batch equilibrium melting trends for various proportion of clinopyroxene and garnet left in the solid residue, for different degrees of partial melting (D'Orazio et al., 2001). Because Yb is compatible in garnet, whereas La and Sm are incompatible, La/Sm and Sm/Yb will be strongly fractionated when melting degree is low. In contrast, La/Sm is

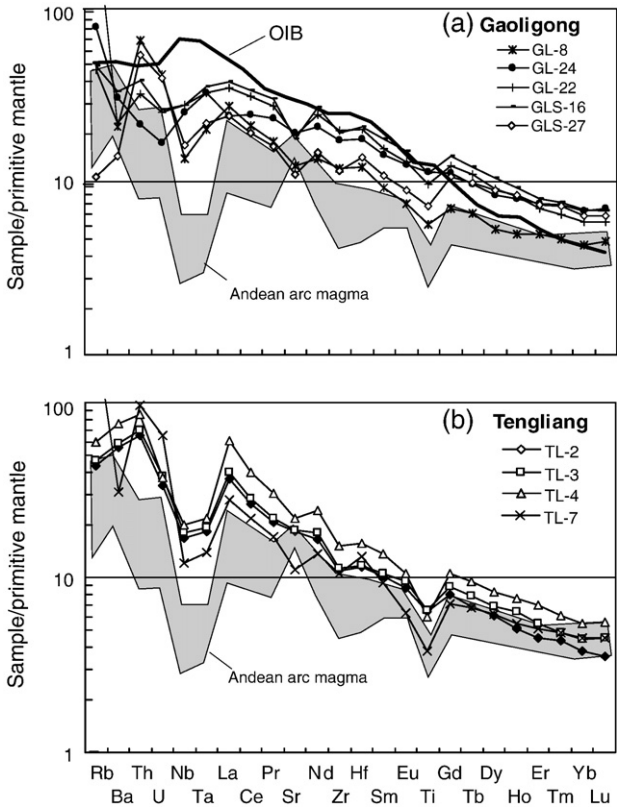


**Fig. 6.** Primitive mantle-normalized incompatible trace-element variation diagrams for the Gaoligong–Tengliang mafic dykes. The range of Andean arc andesites is constructed using data from GEOROC (www.georoc.com). The composition of oceanic island basalts and the normalizing values are from Sun and McDonough (1989).

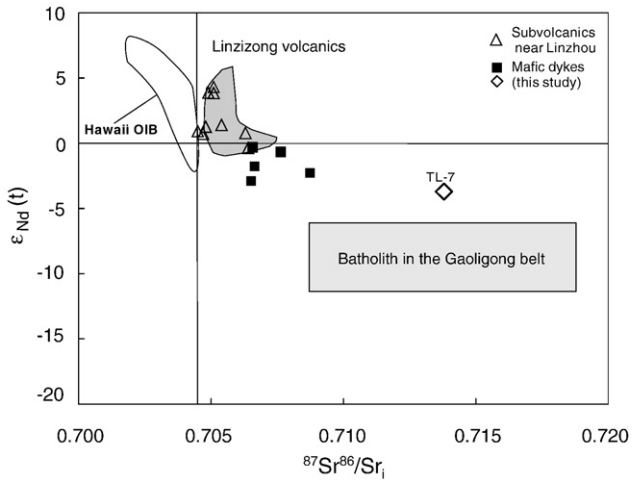


**Fig. 7.** Initial $\varepsilon_{Nd}$ versus $^{87}Sr/^{86}Sr$ of the Gaoligong–Tengliang mafic dykes. Data for the Linzizong volcanics and Gaoligong batholiths are from Mo et al., 2007) and Yang et al. (2006), respectively.

only slightly fractionated and Sm/Yb is nearly unfractionated during the melting in the spinel stability field. It is noted that the Gaoligong–Tengliang mafic dykes are plotted within the melting trends with no to low content of garnet (Cpx:Grt=6:1) in source, suggesting that variable degrees (1–10%) of batch melting of a hypothetical mantle source with small amount of garnet can generate the La/Yb–Sm/Yb systematics of the studied rocks. This is further confirmed by Fig. 10b, in which the Gaoligong–Tengliang rocks can be viewed as mixture of melts derived from a garnet-bearing mantle and a spinel-bearing source. The relatively low Dr/Yb and La/Yb suggest that the Gaoligong samples are dominantly from the spinel facies mantle (>95%). Therefore, it can be inferred that the Gaoligong basalts were generated at a relatively shallow depth, mostly within the spinel stability field. If the concept of the melting column (Langmuir et al., 1992) applies and the depth of the spinel to garnet transition at the peridotite solidus is assumed at ~75–80 km following McKenzie and O'Nions (1991) and Robinson and Wood (1998), this implies that the decompressing asthenosphere rose to a relatively shallow level (<80 km).

Previous evaluation suggests that the Gaoligong dykes represent the asthenosphere-derived melts which has been contaminated to various degree by the lithosphere mantle-derived melts, while the Tengliang samples represent lithosphere mantle-derived melts. This raises the question as to whether the composition of contaminated asthenospheric melts can still be used to infer the melting condition. The two suites show similar REE patterns with the Tengliang samples having slightly lower HREE than the Gaoligong dykes (Fig. 6). It is thus conceivable that the contamination by CLM-derived melts will result in lowering in HREE contents in the asthenospheric magmas. Such a contamination will increase Dy/Yb and La/Yb ratios, which can be translated to slight overestimation of melting depth for the Gaoligong samples. Clearly, this does not affect our inference for a shallow asthenospheric mantle source.

### 5.4. Triggers of intraplate-type magmatism in convergent zone

Any proposed geodynamic model must explain the following characteristics of the Gaoligong–Tengliang mafic dykes: (1) intraplate-type geochemical affinity; (2) small volume; (3) tight time span of magmatism, and (4) the temporal coincidence with a number of geologic events in Tibet. The intraplate-type geochemical characteristics of the Eocene Gaoligong–Tengliang samples require upwelling of the convective asthenosphere to a relatively shallow level (<80 km). The shallow asthenospheric source is in great contrast with the

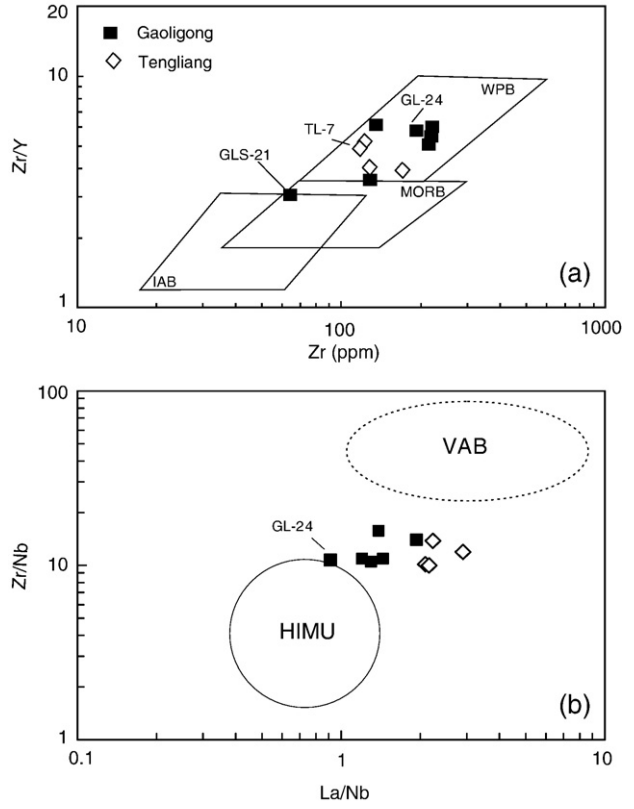


**Fig. 8.** (a) Zr/Y versus Zr, (b) Zr/Nb versus La/Nb for the Gaoligong–Tengliang mafic dykes. Discrimination fields of within plate, MORB and island arc basalts in (a) are after Pearce (1982). Fields of VAB and within-plate basalts in (b) are from Macera et al. (2008).

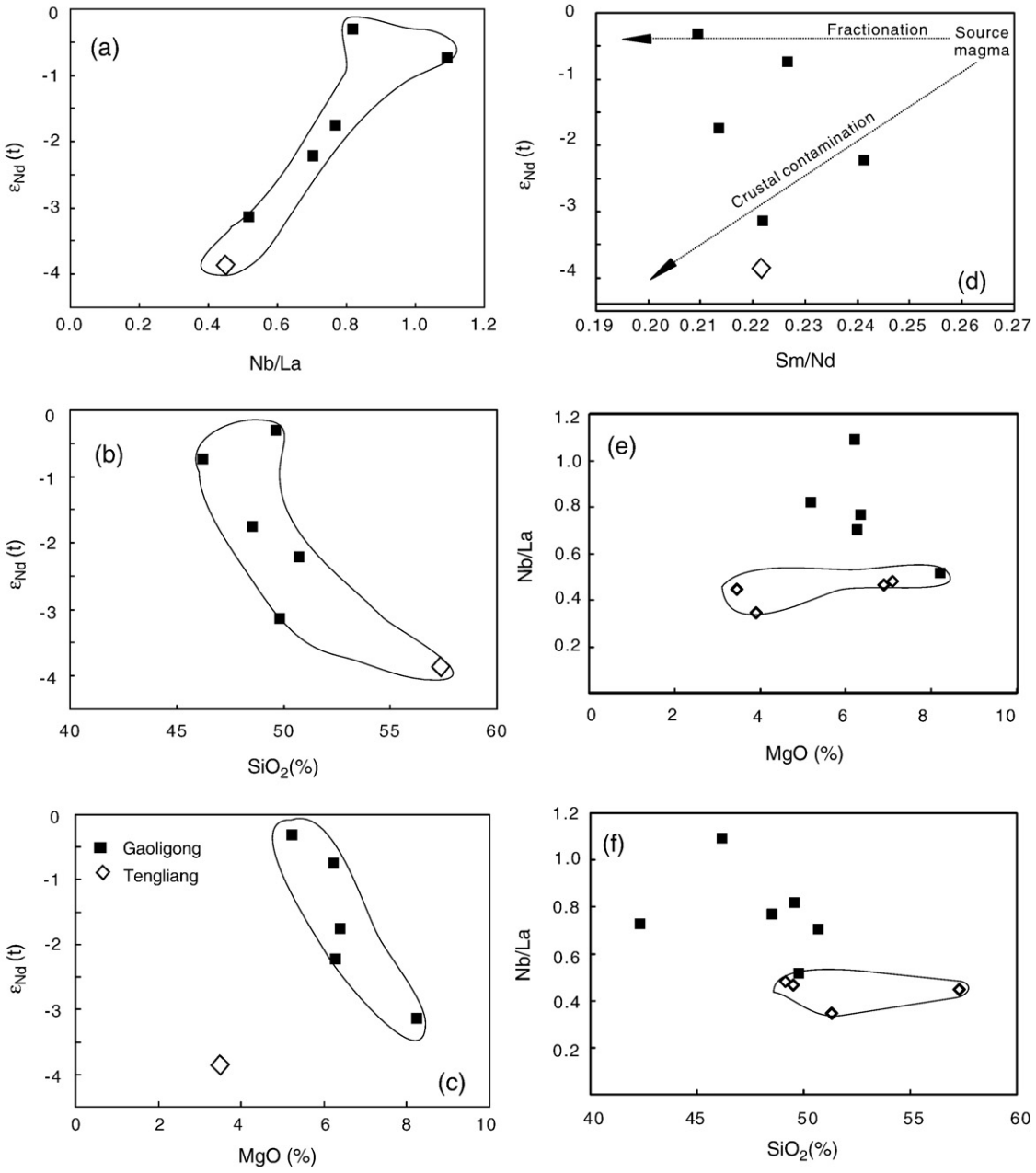


**Fig. 9.** Plot of $\varepsilon_{Nd}(t)$ against (a) Nb/La, (b) $SiO_2$, (c) MgO and (d) Sm/Nd for the Gaoligong–Tengliang mafic dykes. Plot of Nb/La against (e) MgO and (f) $SiO_2$.

current thick lithosphere beneath the Tibetan Plateau (>120 km; Meissner et al., 2004). This contradiction implies that the lithosphere during the Eocene either was not as thick as in modern time, or had somehow been thinned. It remains controversial as to when lithospheric thickening took place in Tibet. Appearance of ~80 Ma adakitic intrusions (Wen et al., in press) and adakite-like rocks in the Pana (Linzizong) rhyolitic succession (50–40 Ma) (Mo et al., 2007) implies the presence of garnet as a residual phase in the mantle source. Therefore, the lithosphere may have already been thickened before 40 Ma, a condition that would prevent the asthenosphere from arising and melting. According to McKenzie and Bickle (1988), dry asthenosphere can melt only when the lithosphere is sufficiently thinned (<70–80 km). Consequently, the occurrence of the intraplate-type magma suggests that the lithosphere in Tibet was locally thinned to certain extent so that decompression melting of the asthenosphere could happen. This demands a dynamic mechanism that is able to thin the lithosphere in orogenic context. At least three competing mechanisms can be envisaged: (1) delamination due to the gravity-induced collapse of the orogenic root during late orogenic extension (Gardien et al., 1997); (2) convective thinning of the lithospheric root (Houseman et al., 1981) and (3) slab break-off affecting the lithospheric structure in orogenic belt (von Blanckenburg and Davies, 1995).

The delamination due to the gravity-induced collapse of the orogenic root would bring the asthenosphere into contact with the Moho. This induces intensive crustal melting and decompressional melting of the asthenosphere if the crust is not very thick (Turner et al., 1999). Although crustal melting occurred in the studied area, the granitic plutons were mainly emplaced in the late Cretaceous (66–76 Ma) and Paleogene (50–55 Ma) (Xu et al., submitted for publication). These crustal melting events thus predated considerably the asthenosphere upwelling-induced intraplate magmatism.

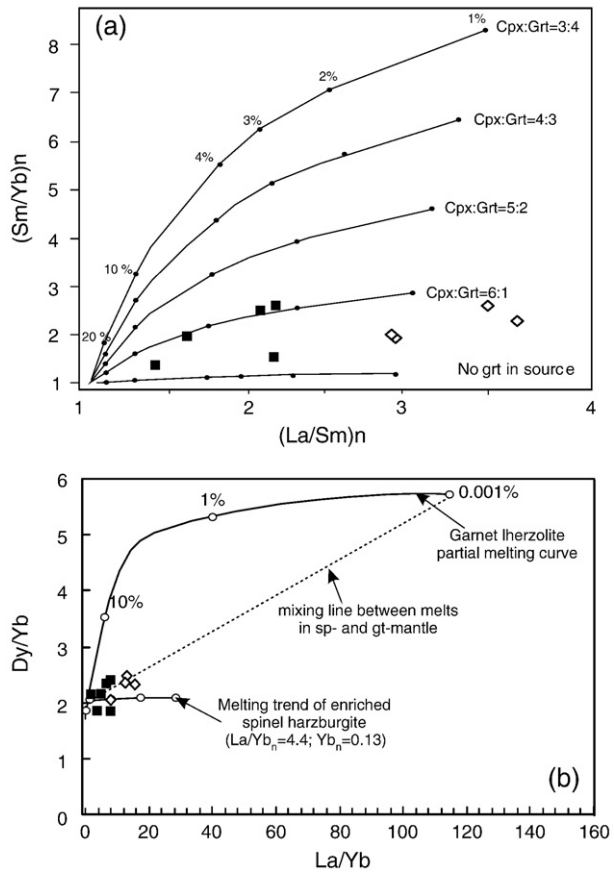


**Fig. 10.** (a) Sm/Yb versus La/Sm diagram for the Gaoligong mafic dykes. Batch melting trends for various clinopyroxene/garnet ratios in the residue solid are taken from D'Orazio et al. (2001); (b) variation of La/Yb and Dy/Yb. The melting model, mode and partition coefficients are after Xu et al. (2001).

Negative $\varepsilon_{Hf}$ (−12 to −4) in zircon from the Gaoligong–Tengliang batholiths further indicate a predominant Proterozoic sedimentary source for the crustal melts with little mantle contribution (Xu et al., submitted for publication), a feature inconsistent with delamination-induced crustal melting. Therefore, if massive crustal melting is the hallmark of delamination, we find little evidence for it in the Gaoligong–Tengliang area. Another prediction of the delamination model is widespread, intensive asthenosphere-derived magmas. Although the volume of intraplate-type magmas in Tibet is poorly constrained at present, available data suggest that it is rather limited. In addition to the Gaoligong dykes, magmatism of similar ages with potential involvement of asthenospheric components is only documented in the sub-volcanic dykes in the Dazi basin, southern Lhasa Terrane (Gao et al., in press). Given the limited occurrence of OIB-type magmatism at the Eocene and the general lack of coeval large-scale crustal melting, the delamination model seems inappropriate in the Gaoligong case.

In the case of convective thinning, as the lithosphere is progressively heated from below, the lower boundary layer of the mechanical lithosphere melts, followed by the shallower lithospheric mantle (Turner et al., 1999). Whether decompression melting of the asthenosphere occurs depends on the level to which the asthenosphere rises (McKenzie and Bickle, 1988). Therefore, progressive decreasing in melting depth and transition in magma source from the lithosphere mantle to the asthenosphere are expected with the convective thinning model. In the present study, the 42 Ma Tengliang dykes, predominately derived from the enriched lithospheric mantle, have relatively lower HREE contents (Yb=1.8–2.7 ppm, i.e., relatively deep melting depth) than the ~40 Ma Gaoligong dykes (Yb=2.9–3.4 ppm, except for GL-8 which has Yb=2.1 ppm), which represent asthenospheric melts contaminated by CLM-derived melts. This magmatic evolution pattern seems consistent with the prediction by the convective thinning model. However, in a broader time scale, the ~40 Ma intraplate-type magmatism in Tibet was predated by the Linzizong volcanism which is characterized by calc-alkaline affinity and overwhelmingly depleted isotopic composition (Mo et al., 2007), rather than an enriched isotopic signature as would be expected by the convective removal model. There is a consensus that the Linzizong volcanic rocks represent arc magmatism related to the corner convection induced by rollback of the Neo-Tethyan plate (Ding et al., 2003; Chung et al., 2005). In this sense, the transition from Cretaceous–early Tertiary subduction-related magmatism to the Eocene intraplate type is inconsistent with the prediction by the convective removal model. Moreover, convective thinning is likely in a large scale, resulting in diffusive and widespread volcanism, a prediction un-matched by the limited volume of the Eocene intraplate magmatism in Tibet.

In the slab break-off model, the detachment of a lithospheric slab allows the asthenosphere underlying the downgoing plate to flow up into the broken slab window above the sinking slab. The heat supply from the uprising asthenosphere can affect overlying lithosphere, yielding characteristic magmatic evolution trend. Asthenosphere upwelling will induce partial melting of the overlying lithospheric mantle previously metasomatized during subduction. If the detachment occurs at shallow depth, decompression melting of the asthenosphere can take place (von Blanckenburg and Davies, 1995). Thermal flux can cause crustal melting and heated crust facilitates the involvement of crustal components within mantle-derived melts through assimilation–fractionation–crystallization processes. Hence, the slab break-off model predicts a magmatic evolution pattern similar to that envisaged by the convective thinning model. However, unlike the diffusive and widespread pattern in the convective thinning case, slab detachment predicts a narrow, linear zone of magmatism of limited extent.

Limited occurrence of the intraplate magmas does not allow the definition of magmatic pattern in Tibet, in particular with respect to the Yarlung-Tsanpo suture. The studied dykes were collected from late Cretaceous-Paleogene granites, which are located distal to the Bangong-Nujiang suture but proximal to the Gangdese belt (Xu et al., submitted for publication). The sub-volcanic dykes in Dazi basin (southern Lhasa) show similar emplacement age and geochemistry to the Gaoligong dykes (Gao et al., in press). All these suggest that the sporadic intraplate magmas likely run parallel the Gangdese belt.

The preference of the Eocene slab break-off model over other models is also built on the close temporal correlation between the intraplate-type magmatism and a number of geologic events/observations in southern Tibet, including the termination of Gangdese arc magmatism (Chung et al., 2005; Mo et al., 2007), the onset of the rapid cooling of the Gangdese batholiths (He et al., 2007), thermal metamorphism (e.g., Kohn and Parkinson, 2002; DeCelles et al., 2002) and geochemical contrast between pre-40 Ma and post-40 Ma magmatism in Tibet. As will be demonstrated in the following section, these characteristics are consistent with the major predictions by the slab break-off model (von Blanckenburg and Davies, 1995).

### 5.5. Other evidence for an Eocene slab break-off model

#### 5.5.1. Termination of the Gangdese arc magmatism

The Gangdese arc-related magmatism ceased no later than ~40 Ma and since that time igneous rocks of calc-alkaline geochemical affinities have not been emplaced in southern Tibet. Therefore, the Gangdese magmatism marked the termination of subduction of oceanic lithosphere (Chung et al., 2005). The emplacement age of the Gaoligong–Tengliang dykes is roughly the same as that of the youngest Gangdese arc magmatism (Zhou et al., 2004; Chung et al.,

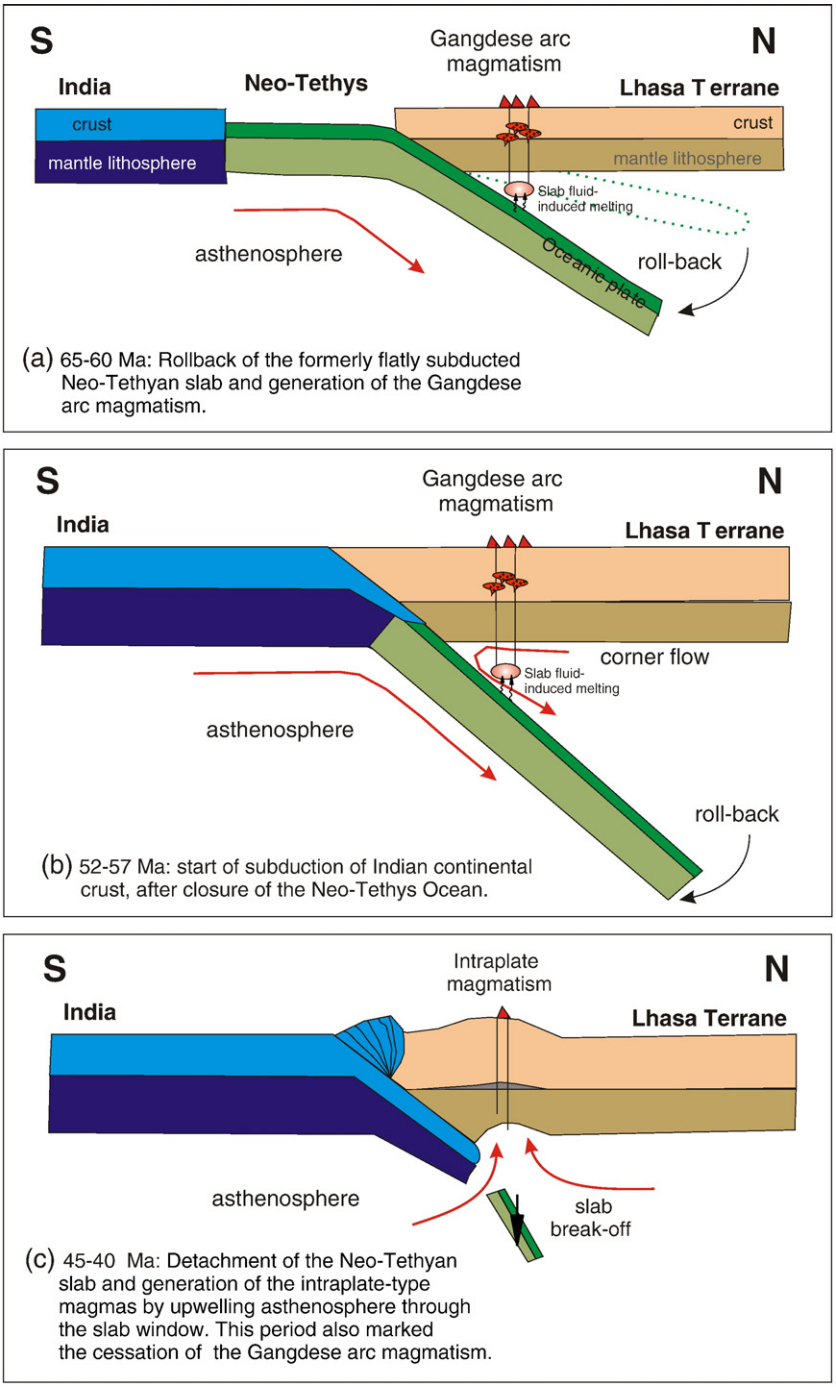


**Fig. 11.** Diagram illustrating tectonic evolution in Tibetan plateau (modified after Chung et al., 2005). (a) 65–60 Ma: rollback of the formerly flatly subducted Neo-Tethyan slab and generation of the Gangdese arc magmatism. (b) 52–57 Ma: arrival of the Indian continent at the trench leading to the closure of the Neo-Tethys Ocean. During this period, the Gangdese arc magmatism continued because of the enhanced corner flow due to slab rollback. (c) 45–40 Ma: detachment of the Neo-Tethyan slab and generation of the intraplate-type magmas by upwelling asthenosphere through the slab window. This period also marked the cessation of the Gangdese magmatism, and thermal metamorphism.

2005; He et al., 2007; Fig. 2). This coincidence can be understood as the slab detachment prevented the further participation of slab in magma generation. In the study area, there is a westward migration of continental arc magmatism from the late Cretaceous to the Paleogene, accompanied by an increase in zircon $\varepsilon_{Hf}$ towards the plutons near the China-Burma boarder (Xu et al., submitted for publication). The latter reflects the influence of subduction-related arc belt, which is likely located within Burma. When the rotation of the study area relative to the Lhasa terrane is taken into account, this magmatic pattern in the Gaoligong–Tengliang area corresponds to the southward migration of magmatism in the Lhasa Terrane (Wen et al., 2008). This magma migration has been interpreted as a result of slab rollback, which had been accompanied by a southward migration of the asthenospheric convection beneath Tibet (Ding et al., 2003; Chung et al., 2005; Wen et al., 2008; Fig. 11a). A natural consequence of this slab rollback is the break-off of the subducted oceanic slabs owing to gravitational settling (Wortel and Spakman, 2000).

*5.5.2. Onset of the rapid cooling of the Gangdese batholiths*

Thermal flux lowered the density of the remnant lithosphere thus triggering an uplift of the lithosphere of limited extent (von Blanckenburg and Davies, 1995). This contrasts with the large-scale uplift and

widespread volcanism envisaged in the convective thinning model. Recent thermotectonic modeling (He et al., 2007) reveals the rapid cooling of the Gangdese granitic batholiths starting from ~42 Ma (Fig. 2). He et al. (2007) attributed this rapid cooling to initial stage of syn-collisional thrusting in southern Tibet or to uplift and erosion in response to delamination of the lower crust and mantle lithosphere or to Neo-Tethyan oceanic lithosphere break-off. Although the distinction between these alternatives is not straightforward, the delamination and break-off models are favored here because the onset of rapid cooling is remarkably coincident with the occurrence of intraplate-type magmas, and syn-collisional thrusting cannot yield intraplate-type magmas.

*5.5.3. Eocene thermal metamorphism*

In addition to crustal and mantle melting, the thermal flux associated with upwelling asthenosphere through the slab window would cause thermal metamorphism of preexisting rocks (von Blanckenburg and Davies, 1995; Mahéo et al., 2002). This is actually documented in the Himalayan metamorphic record (e.g., Ding et al., 2001; Kohn and Parkinson, 2002; DeCelles et al., 2002). Ding et al. (2001) have investigated the high pressure granulites exhumed in Namche Barwa (Eastern Himalayan Syntaxis), which have a Gangdese arc affinity. Based on U–Pb zircon dating, they showed that these granulites have experienced high pressure metamorphism at ca. 40 Ma (Ding et al., 2001). A similar Eocene thermal metamorphism has been deduced by Kohn and Parkinson (2002) on eclogites from southeastern Tibet. Given the coincidence with the intraplate-type magmatism identified in this study and by Gao et al. (in press), this granulite-facies metamorphism likely recorded thermal flux from uprising asthenosphere through a slab window.

*5.5.4. Geochemical difference between pre-40 Ma and post-40 Ma magmas*

As illustrated in Fig. 2, most of the pre-40 Ma magmas in southern Tibet are characterized by positive $\varepsilon_{Nd}$ values and calc-alkaline affinity, whereas most of the post-40 Ma magmas are characterized by high potassic contents and negative $\varepsilon_{Nd}$. In particular, the ultrapotassic rocks located to west of the longitude of 87°E in the Lhasa Terrane show Sr–Nd isotopic composition that resembles that of the Indian continental basement (Zhao et al., 2003; Guo et al., 2007). Such a temporal variation in magma composition and possibly in magma source can be correlated to the tectonic evolution in this area. The pre-40 Ma magmas were likely related to the subduction of the Neo-Tethyan oceanic plate underneath the Lhasa Terrane. On the other hand, the involvement of the Indian continental component in the post-40 Ma magmas suggests the arrival of the Indian continental plate underneath the Lhasa Terrane since the late Eocene. This magmatic evolution suggests a change from oceanic subduction to continental subduction (Ding et al., 2003) at or slightly earlier than 40 Ma (Fig. 11b). The proposed Eocene slab break-off is in concert with this change because the slab break-off is commonly induced by attempted continental subduction (von Blanckenburg and Davies, 1995; Gerya et al., 2004).

## 6. Implication for the transition from oceanic to continental crust subduction in Tibet

Continental collision commonly involves the attempted subduction of continental passive margin following the subduction of oceanic plate into the trench. The transition from oceanic to continental crust subduction marks the largest discontinuity in an orogenic cycle. In spite of large number of researches in Tibet Plateau, little concensus has been reached as to the timing of this transition. In particular, the initiation age of the India–Asia collision remains a matter of considerable debate, with views ranging from Late Cretaceous (>65 Ma) to as young as Oligocene (34 Ma) (Searle et al., 1987; Rowley, 1996; Yin and Harrison, 2000; Aitchison et al., 2007). The Eocene intraplate magmatism in the Gaoligong–Tengliang area is temporally and geochemically comparable to 38–42 Ma basalts in the Dazi volcanic basin in the eastern segment of the Gangdese belt (Gao et al., in press). The petrogenetic link of these rocks to slab break-off shed some lights on the onset of the India–Asia collision.

Slab break-off is suggested to occur in the early stages of continental collisions (von Blanckenburg and Davies, 1995; Wong et al., 1997), due to a decrease in the subduction rate damped by the positive buoyancy of continental lithosphere subducted to depth. The subduction of continental crust would cause a decrease in negative buoyancy which generates tensional forces within the slab near the continent/ocean transition (von Blanckenburg and Davies, 1995). As a consequence, slab detachment commonly occurs near the leading edge of continental plate (Fig. 11c). This concept suggests that the initiation of the India–Asia collision must have occurred prior to 42 Ma. Although the timing and depth of slab detachment depend upon many controlling parameters (Wong et al., 1997; Gerya et al., 2004), thermo-mechanical modeling of slab detachment shows that the most favorable time interval for slab break-off is within 10–15 Ma, after the arrival of continental material at the trench (Macera et al., 2008). The validity of these modeled values has been confirmed by studies on various orogenic belts. In the Alps, continental subduction occurred at 55–45 Ma, followed by a singular lamprophyric/granitic magmatic pulse and crustal uplift between 43 and 25 Ma, which are diagnostic of slab break-off (von Blanckenburg and Davies, 1995). By combining the age of the ultrahigh pressure metamorphism of the Tso Morari Complex and the high rate of Indian subduction, Leech et al. (2005) suggested 57 Ma as the onset of India–Asia continental collision in NW Tibet, preceding by 10 Ma the slab break-off process (Kohn and Parkinson, 2002). If the break-off of the Neo-Tethyan slab occurred at 42–40 Ma in eastern Tibet, the time at which the Indian continent arrived at the trench (i.e., closure of the Neo-Tethys Ocean) can be estimated at 52–57 Ma (Fig. 11b). Despite the relatively large uncertainty with this estimation, it provides a working model for further researches. The uncertainty can be decreased if the subduction rate and angle are constrained.

## 7. Conclusions

The mafic dykes in the Gaoligong–Tengliang belt, that were emplaced at 40 and 42 Ma, differ from the typical arc magmatism but geochemically resemble the intraplate-type magmas, thus providing the petrological evidence for the Eocene asthenospheric upwelling in the studied area. Their derivation from the shallow upper mantle contrasts with the current thick lithosphere beneath the Tibetan Plateau. Therefore, the ~40 Ma magmatism likely represents the response to specific stage of the Tibetan tectonic evolution. The emplacement of these intraplate-type magmas is temporally coincident with the termination of the Gangdese arc magmatism and regional thermally-driven metamorphism. These, and the geochemical contrast between pre-40 Ma and post-40 Ma magmatism in Tibet, can be well explained by a slab break-off model, in which the intraplate-type magmatism in the Gaoligong–Tengliang belt resulted from partial melting of the upwelling asthenosphere in the course of the break-off of subducting Neo-Tethys slab from the Indian continental plate. This interpretation implies the onset of the India–Asia collision at 52–57 Ma, according to the slab break-off concept and relevant thermo-mechanical modeling.

## Acknowledgement

We thank Y. Liu, X.L. Tu and X.R. Liang for technical assistance with ICP-MS and MC-ICPMS analyses. Financial support from the Chinese Ministry of Science and Technology (2002CB412603), the National Natural Science Foundation of China (40721063; 90714001) and the CAS/SAFEA International Partnership Program for Creative Research Teams are gratefully acknowledged. Drs. S.-L. Chung, L. Farmer and Editor B. Bourdon are thanked for their insightful and constructive reviews that substantially improved the paper.

## References


Aitchison, J.C., Ali, J.R., Davis, A.M., 2007. When and where did Indian and Asian collide? J. Geophys. Res. 112. doi:10.1029/2006JB004706.

Arnaud, N., Vidal, P., Tapponnier, P., Matte, P., Deng, W.M., 1992. The high K2O volcanism of northwestern Tibet: geochemistry and tectonic implications. Earth Planet. Sci. Lett. 111, 355–367.

Chu, M.F., Chung, S.L., Song, B., Liu, D.Y., O'Reilly, S.Y., Pearson, N.J., 2006. Zircon U–Pb and Hf isotope constraints on the Mesozoic tectonics and crustal evolution of southern Tibet. Geology 34, 745–748.

Chung, S.L., Liu, D.Y., Ji, J.Q., Chu, M.F., Lee, H.Y., Wen, D.J., Lo, C.H., Lee, T.Y., Qian, Q., Zhang, Q., 2003. Adakites from continental collision zones: melting of thickened lower crust beneath southern Tibet. Geology 31, 1021–1024.

Chung, S.L., Chu, M.F., Zhang, Y.Q., Xie, Y.W., Lo, C.H., Lee, T., Lan, C.Y., Li, X.H., Zhang, Q., Wang, Y.Z., 2005. Tibetan tectonic evolution inferred from spatial and temporal variations in post-collisional magmatism. Earth Sci. Rev. 68, 173–196.

Coulon, C., Maluski, H., Bollinger, C., Wang, S., 1986. Mesozoic and Cenozoic volcanic rocks from central and southern Tibet: 39Ar–40Ar dating, petrological characteristics and geodynamical significance. Earth Planet. Sci. Lett. 79, 281–302.

Coulon, C., Mehartsi, M., Fourcade, S., Maury, R., Bellon, H., Louni-Hacini, A., Cotton, J., Coutelle, A., Hermitte, D., 2002. Post-collisional transition from calc-alkaline to alkaline volcanism during the Neogene in Irani (Algeria): magmatic expression of a slab breakoff. Lithos 62, 87–110.

Davies, J.H., Von Blanckenburg, F., 1995. Slab breakoff: a model of lithosphere detachment and its test in the magmatism and deformation of collisional orogens. Earth Planet. Sci. Lett. 129, 85–102.

Debon, F., Le Fort, P., Sheppard, S.M.F., Sonet, J., 1986. The four plutonic belts of the trans-Himalaya–Himalaya: a chemical, mineralogical, isotopic and chronological synthesis along a Tibet–Nepal section. J. Petrol. 27, 219–250.

DeCelles, P.G., Robinson, D.M., Zandt, G., 2002. Implications of shortening in the Himalayan fold-thrust belt for uplift of the Tibetan plateau. Tectonics 21. doi:10.1029/2001TC001322.

Ding, L., Zhong, D.L., Yin, A., Kapp, P., Harrison, T.M., 2001. Cenozoic structural and metamorphic evolution of the eastern Himalayan syntaxis (Namche Barwa). Earth Planet. Sci. Lett. 192, 423–438.

Ding, L., Kapp, P., Yin, A., Deng, W.M., Zhong, D.L., 2003. Early Tertiary volcanism in the Qiangtang terrane of central Tibet: evidence for a transition from oceanic to continental subduction. J. Petrol. 44, 1833–1865.

Dong, G.C., Mo, X.X., Zhao, Z.D., Guo, T.Y., Wang, L.L., Chen, T., 2005. Geochronologic constraints on the magmatic underplating of the Gangdise belt in the India–Eurasia collision: evidence of SHRIMP II zircon U–Pb dating. Acta Geol. Sin. 79, 787–794.

D'Orazio, M., Agostini, S., Innocenti, F., Haller, M.J., Manetti, P., Mazzarini, F., 2001. Slab window-related magmatism from southernmost South America: the Late Miocene mafic volcanics from the Estancia Glencross Area (~ 52 S, Argentina–Chile). Lithos 57, 67–89.

Ferrari, L., 2004. Slab detachment control on mafic volcanic pulse and mantle heterogeneity in Central Mexico. Geology, 32, 77–80.

Gao, Y.F., Wei, R., Hou, Z.Q., Wei, R.H., Tian, S., Zhao, R.S., in press. Eocene high-MgO volcanism in southern Tibet: New constraints for mantle source characteristics and deep processes. Lithos.

Gardien, V., Lardeaux, J.M., Ledru, P., 1997. Metamorphism during late orogenic extension: insights from the French Variscan belt. Bull. Soc. Geol. Fr. 168, 271–286.

Gerya, T.V., Yuen, D.A., Maresch, W.V., 2004. Thermomechanical modeling of slab detachment. Earth planet. Sci. Lett. 226, 101–116.

Goto, A., Tatsumi, Y., 1996. Quantitative analyses of rock samples by an X-ray fluorescence spectrometer (II). Rigaku J. 13, 20–39.

Guo, Z., Wilson, M., Liu, J.Q., 2007. Post-collisional adakites in south Tibet: products of partial melting of subduction-modified lower crust. Lithos 96, 205–224.

He, S., Kapp, P., DeCelles, P.G., Gehrels, G.E., Heizler, M., 2007. Cretaceous–Tertiary geology of the Gangdese Arc in the Linzhou area, southern Tibet. Tectonophysics 433, 15–37.

Hirose, K., Kushiro, I., 1993. Partial melting of dry peridotites at high-pressures — determination of compositions of melts segregated from peridotite using aggregates of diamond. Earth Planet. Sci. Lett. 114, 477–489.

Hirschmann, M.M., Kogiso, T., Baker, M.B., Stolper, E.M., 2003. Alkalic magmas generated by partial melting of garnet pyroxenite. Geology 31, 481–484.

Hofmann, A.W., 1997. Mantle geochemistry: the message from oceanic volcanism. Nature 385, 219–229.

Hou, Z.Q., Gao, Y.F., Qu, X.M., Rui, Z.Y., Mo, X.X., 2004. Origin of adakitic intrusives generated during mid-Miocene east–west extension in South Tibet. Earth Planet. Sci. Lett. 220, 139–155.

Houseman, G.A., McKenzie, D.P., Molnar, P., 1981. Convective instability of a thickened boundary layer and its relevance for the thermal evolution of continental convergent belts. J. Geophys. Res. 86, 6115–6132.

Kapp, P., Yin, A., Harrison, T.M., Ding, L., 2005. Cretaceous–Tertiary shortening, basin development, and volcanism in central Tibet. Geol. Soc. Amer. Bull. 117, 865–878.

Kogiso, T., Hirschmann, M.M., Pertermann, M., 2004. High-pressure partial melting of mafic lithologies in the mantle. J. Petrol. 45, 2407–2422.

Kohn, M.J., Parkinson, C.D., 2002. Petrologic case for Eocene slab breakoff during the Indo-Asian collision. Geology 30, 591–594.

Koppers, A.A.P., 2002. ArArCALC — software for 40Ar/39Ar age calculations. Comput. Geosci. 28, 605–619.

Langmuir, C.H., Klein, E.M., Plank, T., 1992. Petrological systematics of mid-ocean ridge basalts: Constraints on melt generation beneath ocean ridges. In: Morgan, J.P., Blackman, D.K., Sinton, J.M. (Eds.), Mantle flow and melt generation at mid-ocean ridges. AGU Geophys Monogr Series, vol. 71, pp. 81–180. Washington DC.

Lee, T.Y., Lawver, L.A., 1995. Cenozoic plate reconstruction of Southeast Asia. Tectonophysics 251, 85–138.

Lee, H.Y., Chung, S.L., Wang, J.R., Wen, D.J., Lo, C.H., Yang, T.F., Zhang, Y.Q., Xie, Y.W., Lee, T. Y., Wu, G.Y., Ji, J.Q., 2003. Miocene Jiali faulting and its implications for Tibetan tectonic evolution. Earth Planet. Sci. Lett. 205, 185–194.

Leech, M., Singh, S., Jain, A.K., Klemperer, S.L., Manickavasagam, R.M., 2005. The onset of India–Asia continental collision: early, steep subduction required by the timing of UHP metamorphism in the western Himalaya. Earth Planet. Sci. Lett. 234, 83–97.

Macera, P.M., Gasperini, D., Ranalli, G., Mahatsent, R., 2008. Slab detachment and mantle plume upwelling in subduction zones: an example from the Italian South-Eastern Alps. J. Geodyn. 45, 32–48.

Mahéo, G., Guillot, S., Blichert-Toft, J., Rolland, Y., Pecher, A., 2002. A slab breakoff model for the Neogene thermal evolution of South karakorum and South Tibet. Earth Planet. Sci. Lett. 195, 45–58.

Martin, H., Smithies, R.H., Rapp, R., Moyen, J.F., Champion, D., 2005. An overview of adakite, tonalit-trondhjemite-granodiorite (TTG), and sanukitoid: relationships and some implications for crustal evolution. Lithos 79, 1–24.

Maury, R.C., Fourcade, S., Coulon, C., et al., 2000. Post-collisional Neogene magmatism of the Mediterranean Maghreb margin: a consequence of slab breakoff. C. R. Acad. Sci. Paris (Earth Planet. Sci.) 331, 159–173.

McKenzie, D.P., Bickle, M.J., 1988. The volume and composition of melt generated by extension of the lithosphere. J. Petrol. 29, 625–679.

McKenzie, D.P., O'Nions, R.K., 1991. Partial melt distributions from inversion of rare earth element concentrations. J. Petrol. 32, 1021–1091.

Meissner, R., Tilmann, F., Haines, S., 2004. About the lithospheric structure of central Tibet, based on seismic: data from the INDEPTH III profile. Tectonophysics 380, 1–25.

Miller, C., Schuster, R., Klötzli, U., Frank, W., Purtscheller, F., 1999. Post-collisional potassic and ultrapotassic magmatism in SW Tibet: geochemical and Sr–Nd–Pb–O isotopic constraints for mantle source characteristics and petrogenesis. J. Petrol. 40, 1399–1424.

Mo, X., Zhao, Z., Deng, J., Flower, M.F., Yu, X., Luo, Z., Li, Y., Zhou, S., Dong, G., Zhu, D., Wang, L., 2006. Petrology and geochemistry of post-collisional volcanic rocks from the Tibetan Plateau: implications for lithosphere heterogeneity and collision-induced asthenospheric mantle flow. In: Dilek, Y., Pavlides, S. (Eds.), Postcollisional Tectonics and Magmatism in the Mediterranean Region and Asia, 409. Geological Society of America Special Paper, pp. 507–530.

Mo, X.X., Dong, G.C., Zhao, Z.D., Guo, T., Wang, L.L., Chen, T., 2005. Timing of magma mixing in the Gangdise magmatic belt during the India–Asia collision: zircon SHRIMP U–Pb dating. Acta Geol. Sin. 79, 66–76.

Mo, X.X., Hou, Z.Q., Niu, Y.L., Dong, G.C., Qu, X.M., Zhao, Z.D., Yang, Z.M., 2007. Mantle contribution to crustal thickening during continental collision: evidence from Cenozoic igneous rocks in southern Tibet. Lithos 96, 225–242.

Pearce, J.A., 1982. Trace element characteristics of lavas from destructive plate boundaries. In: Thorpe, R.S. (Ed.), Andesites. John Wiley, New York, pp. 525–548.

Qiu, H.N., Jiang, Y.D., 2007. Sphalerite 40Ar/39Ar progressive crushing and stepwise heating techniques. Earth Planet. Sci. Lett. 256, 224–232.

Robinson, J.A., Wood, B.J., 1998. The depth of the spinel to garnet transition at the peridotite solidus. Earth Planet. Sci. Lett. 164, 277–284.

Rowley, D., 1996. Age of initiation of collision between India and Asia: a review of stratigraphic data. Earth Planet. Sci. Lett. 145, 1–13.

Schärer, U., Allègre, C.J., 1984. U–Pb geochronology of the Gangdese (trans-Himalaya) plutonism in the Lhasa–Xigaze region, Tibet. Earth Planet. Sci. Lett. 69, 311–320.

Searle, M.P., et al., 1987. The closing of Tethys and the tectonics of the Himalya. Geol. Soc. Amer. Bull. 98, 678–701.

Sun, S.S., McDonough, W.F., 1989. Chemical and isotopic systematics of oceanic basalts: implications for mantle composition and processes. In: Saunders, A.D., Norry, M.J. (Eds.), Magmatism in the Ocean Basins. Geol. Soc. Spel. Pub., vol. 42, pp. 313–345.

Takahashi, E., Kushiro, I., 1983. Melting of a dry peridotite at high pressures and basalt magma genesis. Am. Mineral. 68, 859–879.

Tanaka, T., Togashi, S., Kamioka, H., et al., 2004. JNdi-1: a neodymium isotopic reference in consistency with LaJolla neodymium. Chem. Geol. 168, 279–281.

Turner, S., Hawkesworth, C., Liu, J., Rogers, N., Kelley, S., Van Calsteren, P., 1993. Timing of Tibetan uplift constrained by analysis of volcanic rocks. Nature, 364, 50–53.

Turner, S., Arnaud, N., Liu, J., Rogers, N., Hawkesworth, C., Harris, N., Kelley, S., Van Calsteren, P., Deng, W., 1996. Post-collision, shoshonitic volcanism on the Tibetan Plateau: implications for convective thinning of the lithosphere and the source of Ocean Island basalts. J. Petrol., 37, 45–71.

Turner, S.P., Platt, J.P., George, R.M.M., Kelley, S.P., Pearson, D.G., Novew, G.M., 1999. Magmatism associated with orogenic collapse of the Betic-Alboran domain, SE Spain. J. Petrol. 40, 1011–1036.

von Blanckenburg, F., Davis, J.H., 1995. Slab breakoff: a model for syncollisional magmatism and tectonics in the Alps. Tectonics 14, 120–131.

Wang, Q., McDermott, F., Xu, J.F., et al., 2005. Cenozoic K-rich adakitic volcanic rocks in the Hohxil area, northern Tibet: lower-crustal melting in an intracontinental setting. Geology 33, 465–468.

Wen, D.R., Liu, D.Y., Chung, S.L., Chu, M.F., Ji, J.Q., Zhang, Q., Song, B., Lee, T.Y., Yeh, M.W., Lo, C.H., 2008. Zircon SHRIMP U–Pb ages of the Gangdese batholith and implications for Neotethyan subduction in southern Tibet. Chem Geol. 252, 191–201.

Wen, D.R., Chung, S.L., Song, B.,Iizuka, Y., Yang, H.J., Ji, J.Q., Liu, D.Y., Gallet, S., in press. Late Cretaceous Gangdese intrusions of adakitic geochemical characteristics, SE Tibet: Petrogenesis and tectonic implications. Lithos.

Williams, H., Turner, S.P., Kelley, S., Harris, N., 2001. Age and composition of dikes in Southern Tibet: new constraints on the timing of east–west extension and its relationship to postcollisional volcanism. Geology 29, 339–342.

Wilson, M., 1989. Igneous Petrogenesis: a global tectonic approach. Chapman & Hall, London.

Wong, A., Ton, S.Y.M., Wortel, M.J.R., 1997. Slab detachment in continental collision zones: an analysis of controlling parameters. Geophys. Res. Lett. 24, 2095–2098.

Wortel, M.J.R., Spakman, W., 2000. Subduction and slab detachment in the Mediterranean–Carpathian region. Science 290, 1910–1917.
Wu, F.Y., Huang, B.C., Ye, K., Fang, A.M., 2008. Collapsed Himalaya–Tibetan orogen and the rising Tibetan Plateau. Acta Petrolgica Sin. 24, 1–30.
Xu, Y.G., 2002. Evidence for crustal components in the mantle and constraints on crustal recycling mechanisms: pyroxenite xenoliths from Hannuoba, North China. Chem. Geol. 182, 301–322.
Xu, Y.G., Menzies, M.A., Thirlwall, M.F., Xie, G.H., 2001. Exotic lithosphere mantle beneath the western Yangtze craton: petrogenetic links to Tibet using highly magnesian ultrapotassic rocks. Geology 29, 863–866.
Xu, Y.G., Yang, Q.J., Lan, J.B., Huang, X.L., Luo, Z.Y., Shi, Y.R., Xie, L.W., submitted for publication. Zircon U–Pb age and Hf isotopes of batholiths in Gaoligong–Tengliang belt, eastern Tibet: a comparison with the Lhasa Terrane and tectonic implications. Journal of Geophysical Research.
Xu, R.H., Schärer, U., Allègre, C.J., 1985. Magmatism and metamorphism in the Lhasa block (Tibet): a geochronological study. J. Geol. 93, 41–57.
Yang, Q.J., Xu, Y.G., Huang, X.L., Luo, Z.Y., 2006. Geochronology and geochemistry of granites in the Gaoligong tectonic belt, western Yunnan: tectonic implications. Acta Petrologica Sin. 22, 817–834.
Yin, A., Harrison, T., 2000. Geologic evolution of the Himalayan–Tibetan orogen. Annu. Rev. Earth Planet. Sci. 28, 211–280.
Zhao, Z.D., Mo, X.X., Luo, Z.H., Zhou, S., Dong, G.C., Wang, L.L., Zhang, F.Q., 2003. Subduction of India beneath Tibet: magmatism evidence. Earth Sci. Front. 10, 149–158.
Zhou, S., Mo, X.X., Dong, G.C., Zhao, Z.D., Qiu, R.Z., Guo, T.Y., Wang, L.L., 2004. 40Ar–39Ar geochronology of Cenozoic Linzizong volcanic rocks from Linzhou Basin, Tibet, China, and their geological implications. Chin. Sci. Bull. 49, 1970–1979.